International
Progress Report

IPR-00-28

Äspö Hard Rock Laboratory

TRUE Block Scale Project

Tracer test stage

Interference tests, dilution tests and tracer tests

Peter Andersson
Jan-Erik Ludvigsson
Eva Wass
Magnus Holmqvist

Geosigma AB

October 2000

Svensk Kärnbränslehantering AB
Swedish Nuclear Fuel
and Waste Management Co
Box 5864
SE-102 40 Stockholm Sweden
Tel 08-459 84 00
+46 8 459 84 00
Fax 08-661 57 19
+46 8 661 57 19

Äspö Hard Rock Laboratory

Report no.
IPR-00-28
No.
F56K
Author
Peter Andersson
Jan-Erik Ludvigsson
Eva Wass
Magnus Holmqvist
Date
Oct 2000
Checked by
Anders Winberg
Date
Dec 2000
Approved
Olle Olsson
Date
Dec 2000

Äspö Hard Rock Laboratory

TRUE Block Scale Project
Tracer test stage

Interference tests, dilution tests and tracer tests

Peter Andersson
Jan-Erik Ludvigsson
Eva Wass
Magnus Holmqvist

Geosigma AB

October 2000

Keywords: TRUE, Block Scale, tracer tests, tracer dilution test, interference test

Report no.
IPR-00-28
No.
F56K
Author
Peter Andersson
Jan-Erik Ludvigsson
Eva Wass
Magnus Holmqvist
Date
Oct 2000
Checked by
Anders Winberg
Date
Dec 2000
Approved
Olle Olsson
Date
Dec 2000

Äspö Hard Rock Laboratory

TRUE Block Scale Project
Tracer test stage

Interference tests, dilution tests and tracer tests

Peter Andersson
Jan-Erik Ludvigsson
Eva Wass
Magnus Holmqvist

Geosigma AB

October 2000

Keywords: TRUE, Block Scale, tracer tests, tracer dilution test, interference test

Abstract

This report describes the performance and results of the first phase, Phase A, of the TRUE Block Scale Tracer Test Stage. Phase A included four large-scale pressure interference tests combined with tracer dilution tests and multiple-hole tracer tests in two different flow geometries. The main objective of the tests was to test the connectivity of the target area to serve as a basis for selecting a suitable flow geometry for the planned tracer tests in Phase B and C of the project. The tests generally confirmed the structural model of the target area. The results also served as an input to the final choice of tracer test geometry to be used for the planned tracer tests during Phase B and C of the project.

Executive Summary

Presently the fourth and last of the defined stages, the Tracer Test Stage, has started where the results of the performed characterisation is capitalised in the form of a series of tracer tests in the block scale (L=10-50 m). The first phase, Phase A, was performed with the main objective to test the connectivity of the structures in order to select the best suitable geometry for the planned tracer test in Phase b and C of the Tracer Tests Stage.

The Phase A tests involved five different test set-ups, the four first (A-1 to A-4) with tracer dilution tests combined with pumping and the two last (A-4 and A-5) including multiple-hole tracer tests. The test cycle for the dilution tests in A-1 to A-4 was similar to the one used in the pre-tests PT-1 to PT-4 (Andersson et al., 1999) and in the combined interference and tracer tests performed in the Preliminary Characterisation Stage (PCS) (Andersson et al., 1998). Test A-1 and A-2 included dilution tests in 18 selected sections, whereas tests A-3 and A-4 include 12 and 5 sections, respectively.

Tests A-4 and A-5 were focused on tracer transport and performed in radially converging flow geometry. In test A-4 tracer injections were made in three sections (KI0025F03:P5, KI0025F03:P6 and KI0025F03:P7) with pumping in section KI0023B:P6. In test A-5 the same set-up as in A-1 was decided to use based on the many good flow responses observed during test A-1. Tracer injections were made in five sections (KI0025F02:P3, KI0025F02:P5, KI0025F02:P6, KI0025F03:P6 and KA2563A:S4) with pumping in section KI0025F03:P5 with the same pumping rate as in test A-1. The tracer injections were performed as decaying pulses and samples were continuously withdrawn from the source sections. In one injection, the tracer solution was exchanged with non-traced water in order to obtain a well-defined finite pulse injection (source term), and thus, shorten the tail of the breakthrough curve.

The performed tests generally confirm the reconciled March'99 structural model and the conclusions from the short-term interference tests in KI0025F03 (Gentzschein & Ludvigson, 2000).

Test A-1 and A-3, using section KI0025F03:P5 and KI0025F02:P5 as sinks, shows very good connectivity with the entire fracture system, in particular structures #20, 21, 22, 23 and 6. The tests confirm that both sinks are located in structure #20. The groundwater flow measurements show significant responses in 11 out of 18 measured sections. The most significant flow responses are in general also found in sections with good pressure responses.

Test A-2, performed by flowing section KI0025F03:P4 shows good pressure responses in structures #20, 21 and 6. Large drawdown but delayed responses are also found in sections including structures #13, 22 and 23. The radius of influence (corresponding to a drawdown >1 kPa) is smaller for test A-2 than for A-1 and A-3, possibly indicating less good hydraulic connection within the structure(s) tested. The test confirms that the sink section is located in structure #21. The groundwater flow measurements generally show better responses in structures #21, 19 and 13 than in test A-1 and A-3 but lower

responses in structures #6, 20, 22 and 23 which is in agreement with the structural model. Section KI0023B:P5 also responds very good to test A-2 indicating that this section is well connected to structure #13 and/or #21 which is consistent with previous tests and conclusions by Doe (1999).

Based on the results from test A-1 to A-3, the best sink to use as an alternative to KI0023B:P6 was KI0025F03:P5, which thus was used for test A-5.
The quantitative analysis of the most prominent pressure responses in all tests generally shows a short period o (pseudo)-radial flow transiting to leaky (pseudo-spherical) flow. Towards the end of the flow period, a virtually steady-state flow occurred in all sections analysed (4-7 sections during each test). The parameter values determined for transmissivity, T, storativity, S, hydraulic diffusivity, T/S, and leakage coefficient, K′/b′, were generally within a relatively narrow range.

The tracer dilution tests in 53 different sections showed that the "natural" flow varies quite a lot within the Block Scale rock volume. An extremely high flow rate (11 l/h) was measured in KI0023B:P7 where a short-circuit between structures #6 and #20 exists as previously discussed in Andersson et al. (1999). The flow rates in the other measured sections typically were in the range 0-300 ml/h. There are also variations in the "natural" flow between the different tests for some sections.

The tracer test in A-4 performed by pumping in structure #21 (KI0023B:P6) resulted in tracer breakthrough from two of three injection points. The tests cover Euclidean distances ranging between 14 to 17 m which probably are longer in reality. The tracer mass recoveries are not very high (30-40 %) but a large portion of the tail of the breakthrough curves still remained to be recovered when sampling was finished, and therefore it is likely that the mass recoveries would have increased by another 20-30 %. The numerical modelling using a simple one-dimensional advection-dispersion model was able to fit the breakthrough curves quite well with low standard errors. The transport parameters calculated based on the mean travel times; fracture conductivity, equivalent fracture aperture and flow porosity, are in the same order of magnitude for both flow paths investigated.

The tracer test in A-5 performed by pumping in structure #20 (KI0025F03:P5) resulted in tracer breakthrough from four of five injection points. The tests cover Euclidean distances ranging between 11 to 29 m which probably are longer in reality.

Based on the results from the analysis of the tracer tests performed during tests A-4 and A-5 together with previous tracer tests performed (PT-4, Andersson et al., 1999) a final choice of sink for the planned tracer test during Phase B and C of the Tracer Test Stage was done. The planned tests include injections of radioactive sorbing tracers that require high mass recovery and good control of the experiments. Test A-5 only gives one or maybe two flow paths with high enough mass recovery whereas test A-4, using KI0023B:P6 as sink gave at least four possible injection points. Thus, the latter sink is suggested to use for the planned tracer tests in Phase B and C.

Contents

1 Introduction

1.1 Background

The TRUE Block Scale project is an international partnership funded by ANDRA, ENRESA, Nirex, POSIVA, PNC and SKB (Winberg, 1997). The Block Scale project is one part of the Tracer Retention Understanding Experiments (TRUE) conducted at the Äspö Hard Rock Laboratory. Presently the fourth and last of the defined stages, the Tracer Test Stage, has started where the results of the performed characterisation is capitalised in the form of a series of tracer tests in the block scale (L=10-50 m).

As a final step in the detailed characterisation a series of pre-tests were conducted with the aim to show the feasibility of performing tracer tests in the block scale (Andersson et al., 1999.). The pre-tests together with an update and a reconciliation of the March 99 structural model (Doe, 1999.) have constituted the basis for the planned tracer tests in Phase A of the Tracer Test Stage.

In Winberg, (in prep.) four basic questions are proposed for future tracer tests:

1. What is the conductive geometry of the TRUE Block Scale rock volume? Does the March 1999 structural model (and the results of the subsequent hydraulic reconciliation) reflects the conductive geometry with sufficient accuracy to allow design and perform tracer tests?

2. What are the properties of the fractures and fracture zones that control transport in networks of fractures?

3. How do the retention processes control transport in fracture networks, and how can they be measured in field tracer tests?

Hypotheses are proposed for each of these questions:

1. **The major conducting features of the TRUE Block Scale volume trend NW-SE and are subvertical. Being nearly parallel, they do not form a suitable conductive network. Type 2 features provide connectivity in the area between the two major Type 1 Structures #13 and #20.**

2a. **Intersections have distinctive properties and exert a control on transport in fracture/feature networks. These distinctive properties may make the intersection a preferential conductor, a barrier, or a combination of both. Or alternatively:**

2b. **In-plane heterogeneity and anisotropy control transport of solutes in a block scale fracture network**

3. **Conducting features have distinctive and identifiable properties that affect tracer retention. This retention may also vary with scale due the types of features that tracers encounter along a pathway and their retention properties. At a block scale these variations may reflect the retention behaviours of multiple features and their intersections.**

1.2 Objectives

The primary objective of the Tracer Test Stage is to provide us with the data from which we can "increase understanding, and the ability to predict" "transport in a fracture network" in a block scale, i.e. over a length scale of 10–50 m. In addition, to "assess the importance of tracer retention mechanisms (diffusion and sorption) in a fracture network" (Winberg, in prep.).

The specific objective for each test performed within Phase A and the coupling to the formulated hypotheses are presented in Table 1-1.

Table 1-1. Objectives and hypotheses addressed with phase A tracer tests #1 to #5 (A-1 to A-5). The structural interpretation and notation refers to the March 1999 model (Hermanson, in prep.)

Test #	Type of test and sink employed	Objective	Hypotheses tested
A-1	Dilution tests, sink in KI0025F03:P5	Test of connectivity (flow and pressure responses) between structure #20 in KI0025F03 and 18 selected sections in the borehole array	1,2
A-2	Dilution tests, sink in KI0025F03:P4	Test of connectivity (flow and pressure responses) between structure #21 in KI0025F03 and 18 selected sections in the borehole array	1,2
A-3	Dilution tests, sink in KI0025F02:P5	Test of connectivity (flow and pressure responses) between sink in KI0025F02:P5 (structure #20) and 5 structures in KI0025F03	1
A-4	Dilution tests and cross-hole tracer test, sink in KI0023B:P6	Complementary dilution tests and test of transport connectivity, assessment of transport properties using KI0023B:P6 (structure #21) as sink	1, 3
A-5	Cross-hole tracer test, sink in best alternative sink	Test of transport connectivity, assessment of transport properties using alternative sink. Prediction case for modelling	1, 2, 3

2 Performance and evaluation procedure

2.1 Equipment and tracers used

Each of the five characterisation boreholes involved in the tests is instrumented with 6-10 inflatable packers such that 5-10 borehole sections are isolated. Each borehole section is connected to a pressure transducer which is connected the HMS-system. Each of the sections planned to be used for tracer tests are equipped with three nylon hoses, two with an inner diameter of 4 mm and one with an inner diameter of 2 mm. The two 4-mm hoses are used for injection, sampling and circulation in the borehole section whereas the 2-mm hose is used for pressure monitoring.

The tracer dilution tests were performed using six identical equipment set-ups for tracer tests, i.e. allowing six sections to be measured simultaneously. A schematic drawing of the tracer test equipment is shown in Figure 2-1. The basic idea is to have an internal circulation in the borehole section. The circulation makes it possible to obtain a homogeneous tracer concentration in the borehole section and to sample the tracer concentration outside the borehole in order to monitor the injection rate of the tracer with time, and also the dilution rate.

Circulation is controlled by a pump with variable speed (A) and measured by a flow meter (B). Water and tracer injections are made with two different HPLC plunger pumps (C1 and C2) and sampling is made by continuously extracting a small volume of water from the system through a flow controller (constant leak) to a fractional sampler (D). Water and tracer solution is stored in two separate pressurised vessels (E1 and E2) under nitrogen atmosphere. The tracer test equipment has earlier been used in the TRUE-1 tracer tests (e.g. Andersson, 1996).

The tracers used were four fluorescent dye tracers, Uranine (Sodium Fluorescein) from KEBO (purum quality), Amino G Acid from Aldrich (techn.quality), Rhodamine WT from Holiday Dyes Inc. (techn. quality) and Naphtionate from Fluka (purum quality). These tracers, except Naphtionate, have all been used extensively in the TRUE-1 tracer tests and in the TRUE Block Scale Pre-tests.

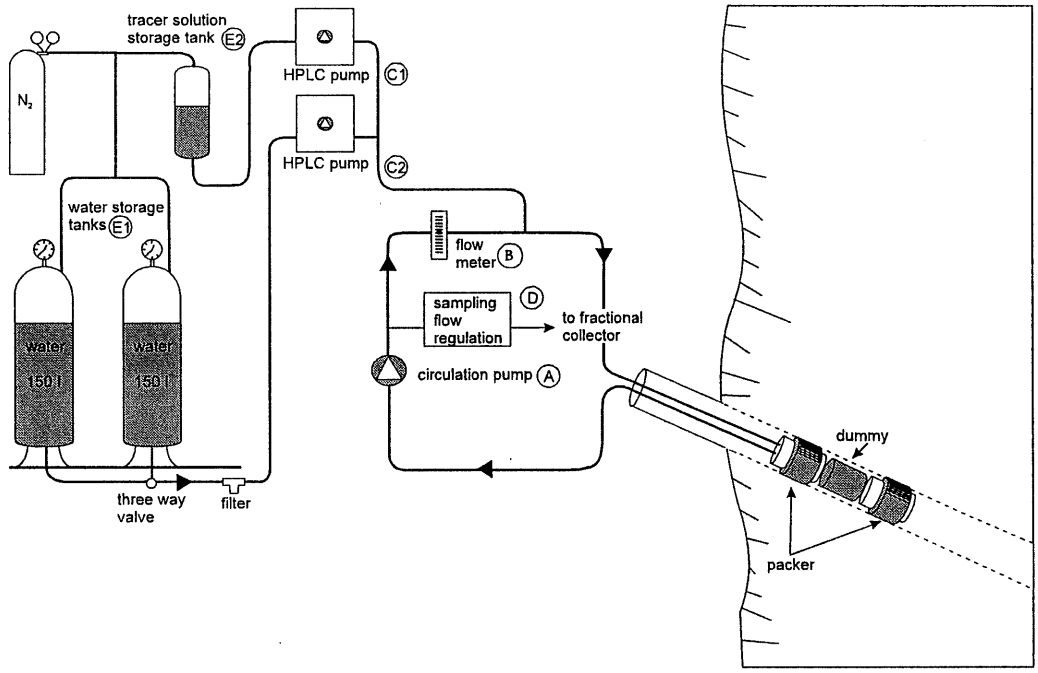

Figure 2-1. Schematic drawing of the tracer injection/sampling system used in the TRUE Project.

2.2 Performance of the Phase A interference tests, dilution tests and tracer tests (A-1, A-2, A-3, A-4 and A-5)

The Phase A tests involved five different test set-ups, the four first (A-1 to A-4) with tracer dilution tests combined with pumping and the two last (A-4 and A-5) including multiple-hole tracer tests, cf. Table 1-1.

The test cycle for the dilution tests in A-1 to A-4 was similar to the one used in the pre-tests PT-1 to PT-4 (Andersson et al., 1999) and in the combined interference and tracer tests performed in the Preliminary Characterisation Stage (PCS) (Andersson et al., 1998). Test A-1 and A-2 included tests in 18 selected sections and had a test cycle of seven days (pumping period 67-71 hours) compared to maximum 12 sections in the pre-tests (and test A-3) with a cycle of five days (pumping period 46 hours). The following test cycle was used:

Day 1	start tracer dilution test under natural gradient in six selected sections
Day 2	change of test sections to six new locations
Day 3	start pumping in selected sink section
Day 4	change of test sections to the six first tested
Day 5	change of test sections to six new locations (only A-1 and A-2)
Day 6	stop pumping
Day 7	stop dilution test in the six selected sections (only A-1 and A-2), preparations for the next test

The dilution tests in A-4 only included five sections with a duration of three days each and hence, a duration of the pumping period of 24 hours, cf. Table 2-1. The tracer test A-5 did not include any measurement during unstressed conditions. Instead the actual injection of tracers was preceded by a period of one day with pumping in the selected sink section to establish stationary flow and pressure conditions.

The withdrawal flow was established using 75 % of the maximum sustainable flow rate during the first five hours of pumping of tests A-1 to A-4. After five hours the flow rate was increased to the maximum sustainable. In A-5 the sink was established using only maximum possible flow. The dimension of the tubing and the hydraulic transmissivity of the section then only restricted the flow. The reasons for using two withdrawal flow rates were to improve the data quality by using constant flow regulation at early times and to improve the possibility of assessing the flow direction from the tracer dilution tests by having two strengths of the sink.

The pumping and recovery phases were performed as conventional constant head interference tests implying that the flow rates and pressures were monitored with a high measurement frequency. The logging frequency was set to enable transient evaluation of pressure data. This means a logging frequency of one scan every second during the first ten minutes, one scan every minute up to two hours and one scan every ten minutes up to two days.

The flow from the pumped section together with the electrical conductivity of the pumped water were measured manually during the pumping period.

Tests A-4 and A-5 were focused on tracer transport and performed in radially converging flow geometry. In test A-4 tracer injections were made in three sections (KI0025F03:P5, KI0025F03:P6 and KI0025F03:P7) with pumping in section KI0023B:P6. In test A-5 the same set-up as in A-1 was decided to use based on the many good flow responses observed during test A-1. Tracer injections were made in five sections (KI0025F02:P3, KI0025F02:P5, KI0025F02:P6, KI0025F03:P6 and KA2563A:S4) with pumping in section KI0025F03:P5 with the same pumping rate as in test A-1. The tracer injections were performed as decaying pulses and samples were continuously withdrawn from the source sections. In one injection, the tracer solution

was exchanged with non-traced water in order to obtain a well-defined finite pulse injection (source term), and thus, shorten the tail of the breakthrough curve.

Table 2-1 summarises the test set-ups including expected flow rates (based on earlier tests) and distances. The positions of the sinks and sections used for flow measurements using the tracer dilution technique for the different tests are shown in Figures 2-2 to 2-6.

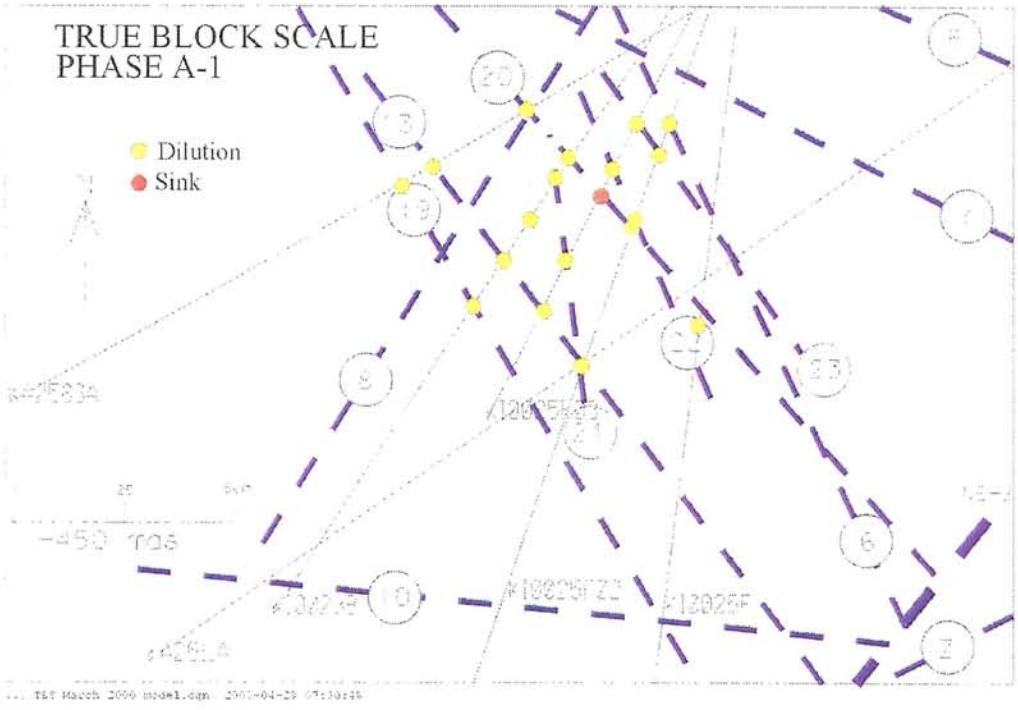

Figure 2-2. Position of sink and dilution test sections during test A-1. The positions of the structures are based on the reconciled March 1999 structural model (Doe, 1999.). Z=-450 masl.

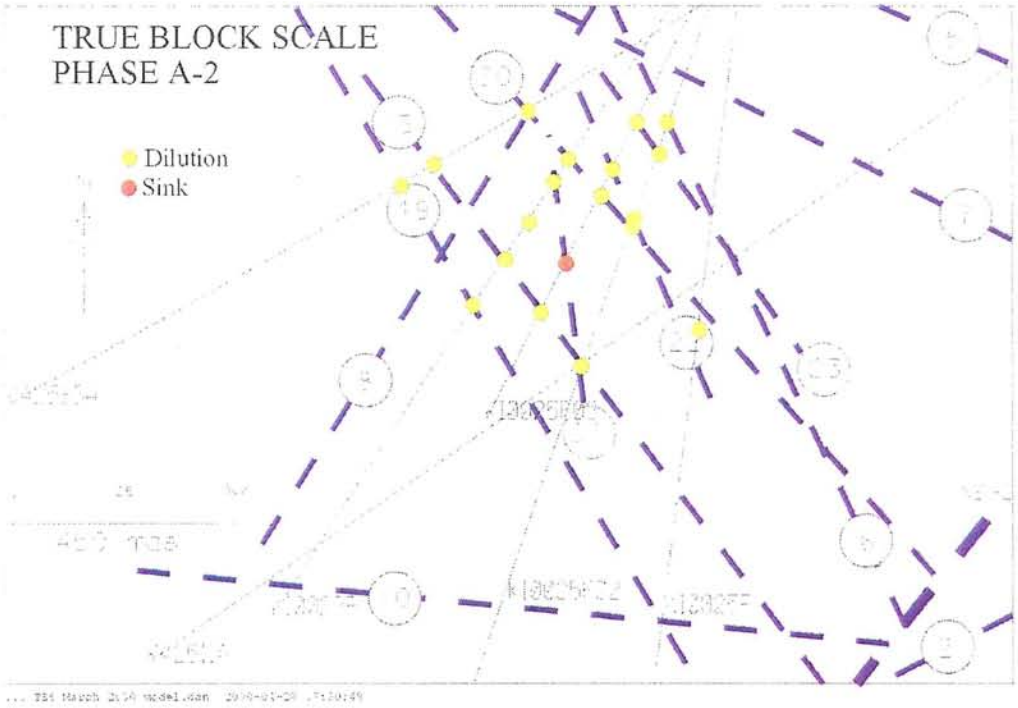

Figure 2-3. Position of sink and dilution test sections during test A-2. The positions of the structures are based on the reconciled March 1999 structural model (Doe, 1999.). Z=-450 masl.

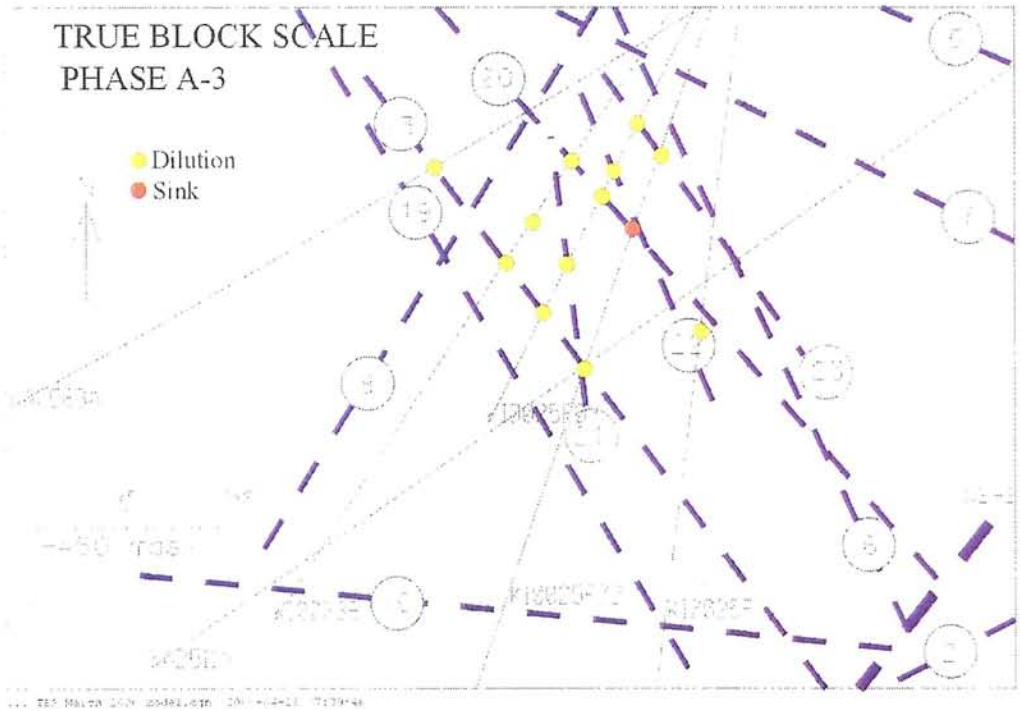

Figure 2-4. Position of sink and dilution test sections during test A-3. The positions of the structures are based on the reconciled March 1999 structural model (Doe, 1999.). Z=-450 masl.

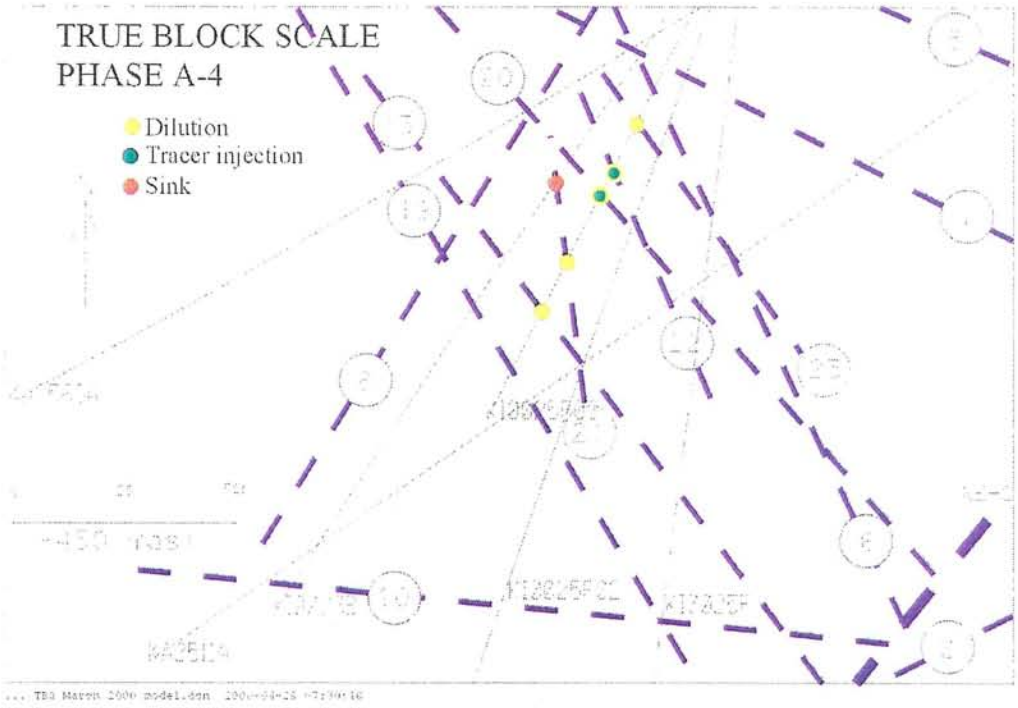

Figure 2-5. Position of sink and tracer injection sections during test A-4. The positions of the structures are based on the reconciled March 1999 structural model (Doe, 1999.). Z=-450 masl.

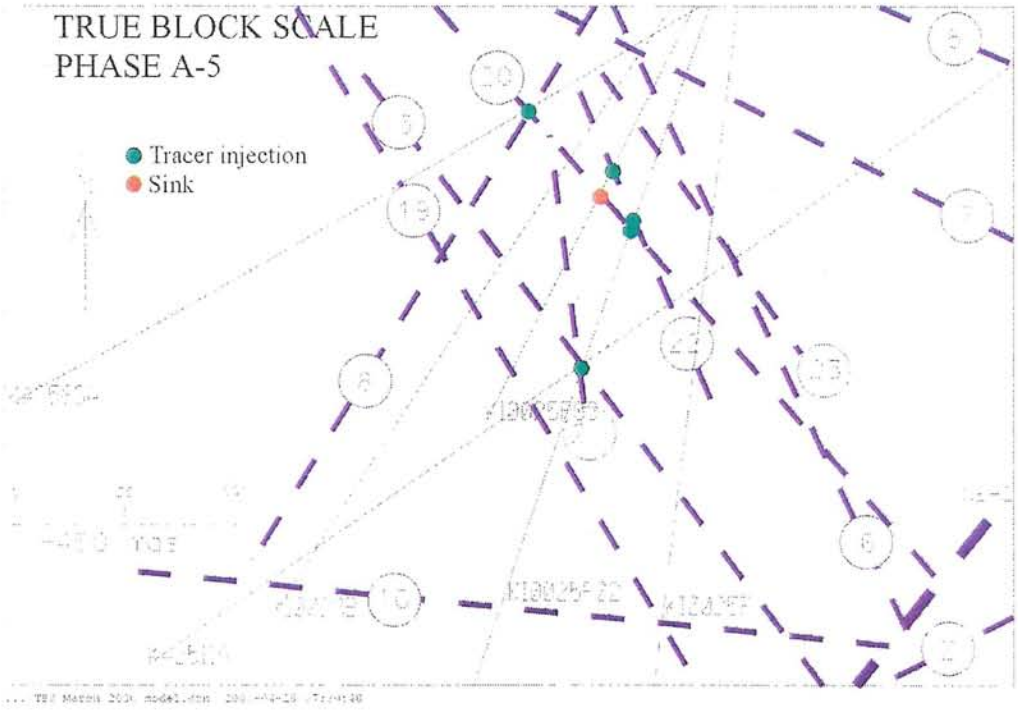

Figure 2-6. Position of sink and tracer injection sections during test A-5. The positions of the structures are based on the reconciled March 1999 structural model (Doe, 1999 .). Z=-450 masl.

Table 2-1. Test set-ups for TRUE Block Scale Tracer Test Stage (TTS), Phase A, tests A-1 to A-5. The structural interpretation and notation refers to the reconciled March 99 model (Doe, 1999).

Test #	Sink	Structure #	Test sections	Structure #	Ambient flow* (ml/h)	Euclidean distance* * (m)	Distance along structures
A-1	KI0025F03:P5	20	KI0025F02:P5	20	50	11	
			KA2563A:S4	20	100	29	
			KI0023B:P7	6, 20	10000	22	
			KI0025F02:P6	22	100	12	
			KI0023B:P4	13	20	18	
			KI0025F02:P3	13, 21	40	26	
			KI0023F03:P3	13	?	18	
			KI0023B:P6	21	3	14	
			KI0025F03:P4	21	?	14	
			KA2563A:S3	13	1	31	
			KI0025F03:P6	22	?	12	
			KI0025F02:P7	23	10	17	
			KA2563A:S1	19	100	52	
			KI0025F:R4	20, 22	1	40	
			KI0023B:P2	19	14	41	
			KI0023B:P5	18	?	15	
			KI0025F03:P7	23	?	26	
			KI0025F02:P8	6	30	23	
A-2	KI0025F03:P4	21	KI0025F02:P5	20	50	17	
			KI0023B:P6	21	3	24	
			KI0023B:P7	6, 20	10000	36	
			KA2563A:S4	20	100	38	
			KI0023B:P4	13	20	17	
			KI0025F02:P3	13, 21	40	16	
			KI0025F03:P3	13	?	4	
			KA2563A:S3	13	1	33	
			KI0025F03:P6	22	?	26	
			KI0025F02:P6	22	100	23	
			KI0025F03:P5	20	?	14	
			KI0025F02:P7	23	10	30	
			KA2563A:S1	19	100	50	
			KI0023B:P2	19	14	29	
			KI0025F:R4	20, 22	1	34	
			KI0023B:P5	18	?	19	
			KI0025F03:P7	23	?	30	
			KI0025F02:P8	6	30	37	

Test #	Sink	Structure #	Test sections	Structure #	Ambient flow* (ml/h)	Euclidean distance* * (m)	Distance along structures
A-3	KI0025F02:P5	20	KA2563A:S3	13	1	39	200
			KI0025F:R4	20, 22	1	23	26
			KI0023B:P4	13	20	22	54
			KI0023B:P5	18	?	20	?
			KI0023B:P7	6, 20	10000	27	27
			KI0025F02:P3	13, 21	40	21	43
			KI0025F02:P7	23	10	16	?
			KI0025F03:P3	13	?	20	
			KI0025F03:P4	21	?	17	
			KI0025F03:P5	20	?	11	11
			KI0025F03:P6	22	?	17	
			KI0025F03:P7	23	?	21	
A-4	KI0023B:P6	21	KI0025F03:P3	13	?	27	
			KI0025F03:P4	21	?	24	
			KI0025F03:P5	20	?	14	
			KI0025F03:P6	22	?	15	
			KI0025F03:P7	23	?	17	
A-5	Best Sink A-1 to A-3	?	?	?	?	?	

* Estimated based on measurements by Andersson et al. (1998, 1999)
** Euclidean distance = shortest geometrical distance

2.3 Laboratory analyses

Samples were analysed for dye tracer content at the GEOSIGMA Laboratory, Uppsala, using a Jasco FP777 Spectrofluorometer.

2.4 Evaluation

2.4.1 Hydraulic interference tests

Qualitative interpretation and pressure response matrix

The hydraulic responses are evaluated in different steps in which part of the data has been sorted out for further (quantitative) evaluation. The qualitative evaluation involves preparation of pressure response diagrams for each test and a common pressure response matrix for all tests. In addition, drawdown versus time-distance diagrams (s versus t/R^2), similar to the pressure response diagrams, and pressure derivative curves are also used in the qualitative evaluation. The latter two methods are described in the quantitative evaluation below.

Time-drawdown (and recovery) plots were prepared for borehole sections showing a total drawdown of more than s_p=0.1 m (1 kPa) at stop of the flow period. This threshold pressure was chosen with consideration of the amplitude of the tidal effects in the boreholes. From these plots, the response times (t_R) for each section were estimated. The response time is here defined as the time after start of flowing when a real drawdown (or recovery) of 1 kPa is observed (from the logarithmic plots) in the actual observation section. The qualitative evaluation has mainly been made on data from the drawdown phase. Data from the recovery phase were used as supporting data.

On the X-axis of the pressure response diagrams, the ratio of the response time (t_R) and the (squared) straight-line distance R between the (midpoint of) the sink section and (the midpoint of) each observation section (t_R/R^2) is plotted. The latter ratio is inversely related to the hydraulic diffusivity of the rock, which indicates the speed of propagation in the rock of the drawdown created in the flowing section.

The final drawdown at stop of flowing (s_p) in the responding sections were determined from the drawdown data. To account for the different flow rates used in the tests and to make the pressure response plots comparable between tests, the final drawdown is normalised with respect to the final flow rate (Q_2). The ratio s_p/Q_2 is plotted on the Y-axis of the pressure response diagrams.

From the response plots of s_p/Q_2 versus t_R/R^2 for each test, sections with anomalous, fast response times (high hydraulic diffusivity) and large (normalised) drawdown can be identified. Such sections, showing primary responses, can be assumed to have a distinct hydraulic connection to the sink section and may be intersected by a single fracture; fracture zones or other conductive structures in the rock. On the other hand, sections with delayed and weak (secondary) responses may correspond to sections in the rock mass between such structures.

From the calculated values of s_p/Q_2 (index 1) and t_R/R^2 (index 2) for each observation section during each test, a common pressure response matrix showing the response patterns for all tests, was prepared by classifying the pressure responses by means of the

above indexes 1 and 2. For index 1, the following class limits and drawdown characteristics were used:

Index 1 (s_p/Q_2)

$s_p/Q_2 > 1 \cdot 10^5$ s/m^2	Excellent (Red)
$3 \cdot 10^4 < s_p/Q_2 \leq 1 \cdot 10^5$ s /m^2	High (Yellow)
$1 \cdot 10^4 < s_p/Q_2 \leq 3 \cdot 10^4$ s /m^2	Medium (Green)
$s_p/Q_2 \leq 1 \cdot 10^4$ s /m^2	Low (Blue)

For index 2 the following class limits and response characteristics were used:

Index 2 (t_R/R^2)

$t_R/R^2 < 0.01$ s/m^2	Excellent (E)
$0.01 \leq t_R/R^2 < 0.1$ s/m^2	Good (G)
$0.1 \leq t_R/R^2 < 0.3$ s/m^2	Medium (M)
$t_R/R^2 \geq 0.3$ s/m^2	Bad (B)

The results from the qualitative analysis of the hydraulic responses were compared with the revised and reconciled structural (March' 99) model and the latter checked for consistency and possible need of revision. It should be pointed out that the response diagrams of s_p/Q_2 versus t_R/R^2 described above were only used as diagnostic tools to identify the most significant responses during each test and to construct the pressure response matrix. The diagrams should be used with some care since the true actual distances (along pathways) between the sink and observation sections are uncertain which may affect the position of a certain point (i.e. section) in the horizontal direction in the diagrams. However, in most cases, the shortest (straight-line) distance between the sink and observation section, as used here, is considered as a sufficient and robust approximation for the above purpose.

Another potential source of error in the response diagrams may occur if (internal) hydraulic interaction exists between sections along an observation borehole. For example, such interaction could either be due to packer leakage (insufficient packer sealing) or rock leakage through interconnecting fractures around the packers. This fact may give a false impression that good hydraulic communication exists between such observation sections and the actual source section. However, any analysis method will suffer from this potential source of error.

Quantitative interpretation

The main purpose of the quantitative interpretation of the interference tests in this study is to estimate the hydraulic parameters and the hydraulic characteristics of the most significant responses, as identified from the previous qualitative interpretation. The estimated hydraulic parameters should represent the hydraulic properties of the dominating fracture zones (or other conductive features) tested. Finally, semi-quantitative evaluation also involved plotting of the most significant responses in a drawdown versus time/distance squared (t/R^2)-diagram.

The derivative of drawdown versus time was used as a diagnostic tool by the deduction of the flow geometry during the test, and thus as a guideline by the quantitative (time-drawdown) analysis, and finally, by the deduction of possible outer hydraulic boundaries. The drawdown derivative was generated by the SKB-code PUMPKONV and plotted together with the drawdown versus time curve.

A combination of the Theis' model for pure radial flow in a non-leaky, porous aquifer (Theis, 1935) and the Hantush model for a leaky aquifer with no aquitard storage (Hantush and Jacob, 1955) was used as standard interpretation models for the quantitative evaluation. The latter model was used because of its generality and its ability to analyse radial as well as leaky (pseudo-spherical) flow. Tests showing well-defined periods with (pseudo-) radial flow were also analysed by Cooper-Jacob's method (Cooper and Jacob, 1946) in semi-logarithmic graphs. The quantitative evaluation was made using the software AquiferTest (Waterloo Hydrologic).

2.4.2 Tracer dilution tests

Flow rates were calculated from the decay of tracer concentration versus time through dilution with natural unlabelled groundwater, c.f. Winberg (*ed*), (1996). The so-called "dilution curves" were plotted as the natural logarithm of concentration versus time. Theoretically, a straight-line relationship exists between the natural logarithm of the relative tracer concentration (c/c_0) and time (t):

$$Q_{bh} = -V \cdot \Delta \ln (c/c_0) / \Delta t \qquad 2\text{-}1$$

where Q_{bh} (m^3/s) is the groundwater flow rate through the borehole section and V (m^3) is the volume of the borehole section. The flow, Q_{bh}, may be translated into a Darcy velocity by taking into account the distortion of the flow caused by the borehole and the angle between borehole and flow direction, c.f. Rhén et al. (1991). The relation between the flow in the rock, the Darcy velocity, q_w (m/s), and the measured flow through the borehole with a dilution test, Q_{bh}, can be expressed as:

$$Q_{bh} = q_w \cdot L_{bh}^2 \left[r_d \cdot \alpha \cdot \sin\beta + \pi \cdot \cos\beta \left(\frac{a_{D1}}{2} + \frac{a_{D2}}{4} + \frac{a_{D3}}{6} \right) \right] \qquad 2\text{-}2$$

where

$$r_d = \frac{2r_w}{L_{bh}} \qquad 2\text{-}3$$

Assuming a 90° angle between borehole and the flow direction the relationship between Q_{bh} and q_w may be estimated from

$$Q_{bh} = q_w \cdot L_{bh} \cdot 2r_w \cdot \alpha \qquad 2\text{-}4$$

where L_{bh} is the length of the borehole section (m), r_w is the borehole radius (m) and α is the factor accounting for the distortion of flow caused by the borehole. The factor α was given the value 2 in the calculations, which is the theoretical value for a homogeneous porous media.

2.4.3 Tracer test

The evaluation of the tracer test has involved computer modelling using a simple one-dimensional advection-dispersion model (Van Genuchten & Alves, 1982). From the computer modelling, dispersivity and mean travel times were determined using an automated parameter estimation program, PAREST (Nordqvist, 1994). PAREST uses a non-linear least square regression where regression statistics (correlation, standard errors and correlation between parameters) also is obtained.

The chosen one-dimensional model assumes a constant fluid velocity and negligible transverse dispersion, cf. Equation 2-5.

$$\partial C/\partial t = D(\partial^2 C/\partial x^2) - v \cdot \partial C/\partial x \qquad 2\text{-}5$$

where: D = Dispersion coefficient
v = fluid velocity (m/s)
C = concentration of solute
x = distance from injection point (m)
t = time (s)

According to Ogata & Banks (1961) and Zuber (1974), the dispersion in a radially converging flow field can be calculated with good approximation by equations valid for one-dimensional flow. Although a linear flow model (constant velocity) is used for a converging flow field, it can be demonstrated that breakthrough curves and parameter estimates are similar for Peclet numbers of about 10 and higher.

Van Genuchten (1982) gives a solution for step input with dispersion over the injection boundary. The solution of Equation 2-5, then is:

$$C/C_o = 2 \text{ erfc } [(x-v \cdot t) / Z] + (V/\pi)^2 \exp [(x-v \cdot t)^2 / (4D \cdot t)] - \qquad 2\text{-}6$$

$$2\,[1+v\cdot x/D+V]\,\exp\,[v\cdot x/D]\,\mathrm{erfc}[(x+v\cdot t)\,/\,Z]$$

where: $Z = 2(D\cdot t)^2$

$V = v^2 t/D$

Variable injection schemes were simulated by superposition of the solution given in Equation 2-6.

The fit of the breakthrough curves using a three-parameter fit included velocity, v, dispersion coefficient, D, and the so called F-factor which corresponds to injected mass divided by fracture volume, M_{inj}/V_f. The result of the evaluation is presented in Chapter 3.6.2 and 3.7.3.

Based on the mean travel times, t_m, determined from the parameter estimation, the hydraulic fracture conductivity, K_{fr} (m/s), were calculated assuming radial flow and validity of Darcy's law (Gustafsson & Klockars, 1981);

$$K_{fr} = \ln (r/r_w)\,(r^2-r_w^2)\,/\,2\cdot t_m\cdot \Delta h \qquad 2\text{-}7$$

where: r = travel distance (m)
r_w= borehole radius (m)
t_m= mean travel time of tracer (s)
Δh= head difference (m)

The equivalent fracture aperture, b (m), was calculated from:

$$b = Q\cdot t_m/\pi\cdot(r^2-r_w^2) \qquad 2\text{-}8$$

where Q (m^3/s), is the mean pumping rate.

Flow porosity, θ_k, was calculated using:

$$\theta_k = K/K_{fr} \qquad 2\text{-}9$$

where K is the hydraulic conductivity of the packed-off section of the borehole determined from steady state evaluation of the interference test (Moye, 1967):

$$K = (Q/\Delta h\cdot L)\cdot((1+\ln L/2r_w)/2\pi) \qquad 2\text{-}10$$

where L (m) is the length of the packed-off section. It should be noted that the term flow porosity might be misleading to use in a fractured heterogeneous rock as it is defined for a porous media. However, it is often used in fractured media as a scaling factor for transport, but then defined over a finite thickness which, in his case, is defined as the length of the packed-off borehole section (L = 1.0 m in test A-4 and 7.5 m in test A-5).

The values calculated using Equations 2-7 through 2-10 are presented together with parameters determined from the numerical modelling of the tracer breakthrough in Table 3-12 (A-4) and Table 3-16 (A-5).

Tracer mass recovery was calculated in two different ways. Common for both methods was that the tracer mass recovered in the pumping borehole was determined by integration of the breakthrough curves for mass flux (mg/h) versus time (h). The injected mass was determined in the same way but also by weighing the tracer solution vessel during the injection procedure.

3 Results and interpretation

3.1 General

The equipment has worked well and no major hydraulic disturbance has occurred during the tests. A few of the sections closest to the I-tunnel have been somewhat disturbed by an unintentional packer deflation in two boreholes in the G-tunnel during the recovery phase of test A-3. However, this has not affected the interpretation of the tests. A summary of the tests is given in Table 3-1.

Table 3-1. Summary of data for tests A-1 to A-5.

Test #	Sink	Structure #	Q_1 (l/min)	Q_2 (l/min)	s_p (m)	Q_2/s_p (m^2/s)	Flow period (h)
A-1	KI0025F03:P5	20	2.05	2.65	249	$1.8 \cdot 10^{-7}$	67
A-2	KI0025F03:P4	21	1.00	1.18	361	$5.4 \cdot 10^{-8}$	71
A-3	KI0025F02:P5	20	3.60	4.10	45.2	$1.5 \cdot 10^{-6}$	46.4
A-4	KI0023B:P6	21	2.05	2.30	190	$2.0 \cdot 10^{-7}$	289.5
A-5	KI0025F03:P5	20	2.60	2.60	237	$1.8 \cdot 10^{-7}$	906

Q_1 = Flow rate during step1 (0-5 h), for test A-3: 0-4 h
Q_2 = Flow rate during step2 (at the end of the flow period)
s_p = Drawdown at the end of the test
Q_2/s_p = Specific capacity

3.2 Pressure response matrix

The pressure response matrix for tests A-1 to A-4 is shown in Figure 3-1 (test A-5 is identical to A-1). The matrix is based on the pressure response diagrams for each test. The colours and letters coding refers to the two indexes s_p/Q (drawdown normalised to pumping rate) and t_R/R^2 (response time normalised to the distance squared) according to Chapter 2.4.1. Index 1 (s_p/Q) is based on the drawdown (larger than 1 kPa) by the end of the flow phase (s_p) and the second flow rate (Q_2) for each test, see Table 3-1.

Figure 3-1 shows that good pressure responses occurred in most of the monitored boreholes during tests #A-1, #A-3 and #A-4. The response patterns during these tests are similar. During test #A-2, fewer sections reacted in the receiver boreholes. The results of the tests are discussed in more detail below.

Sink in Structure		#20	#21	#20	#21	
Borehole	Interval (m)	A-1	A-2	A-3	A-4	Structure
KA2511A:T1	239-293	B		B	B	#10,11,18
KA2511A:T2	171-238	B		B	B	#19
KA2511A:T3	139-170	B		B	B	# ?
KA2511A:T4	111-138	B		B	B	#20
KA2511A:T5	103-110	B		B	B	#16
KA2511A:T6	96-102	B		B	B	#6
KA2511A:T7	65-95	B		B	B	# ?
KA2511A:T8	6-64	B		B	B	#4,7
KA2563A:S1	242-246	B		B	B	#19
KA2563A:S2	236-241	B		B	B	#19
KA2563A:S3	206-208	M	B	G	M	#13
KA2563A:S4	187-190	E	G	E	G	#20
KA2563A:S5	146-186	G	M	G	G	#6,7
KI0025F:R1	169-194			B	B	Z
KI0025F:R2	164-168	B		B	B	#19
KI0025F:R3	89-163	B		B	B	?
KI0025F:R4	86-88	G	M	G	E	#20,22
KI0025F:R5	41-85	B		B	B	#7
KI0025F:R6	3.5-40	B			B	# 5
KI0023B:P1	113.7-200.7				B	#10
KI0023B:P2	111.25-112.7	B		B	B	#19
KI0023B:P3	87.20-110.25	Uncertain				?
KI0023B:P4	84.75-86.20	B	B	M	B	#13
KI0023B:P5	72.95-83.75	G	B	G	E	#18
KI0023B:P6	70.95-71.95	G	M	G	S	#21
KI0023B:P7	43.45-69.95	G	G	E	E	#6, 20
KI0023B:P8	41.45-42.45	B		B	B	#7
KI0023B:P9	4.5-40.45	B			B	#5
KI0025F02:P1	135.15-204				B	#?
KI0025F02:P2	100.25-134.15	B			B	#19
KI0025F02:P3	93.40-99.25	B	B	B	M	#13,21
KI0025F02:P4	78.25-92.4	Tight				#?
KI0025F02:P5	73.3-77.25	G	B	S	G	#20
KI0025F02:P6	64.0-72.3	M	B	M	M	#22
KI0025F02:P7	56.1-63.0	B	B	M	B	#23
KI0025F02:P8	51.7-55.1	G	M	G	G	#6
KI0025F02:P9	38.5-50.7	B		B	B	#7
KI0025F02:P10	3.4-37.5	B			B	#5
KI0025F03:P1	101.0-141.7	B		B	B	#19
KI0025F03:P2	93.5-100.0	B		B	B	?
KI0025F03:P3	89.0-92.5	B	B	B	B	#13
KI0025F03:P4	85.0-88.0	M	S	M	G	#21
KI0025F03:P5	66.5-74.0	S	B	E	G	#20
KI0025F03:P6	59.5-65.5	B	B	M	M	#22
KI0025F03:P7	55.0-58.5	M	B	M	M	#23
KI0025F03:P8	51.5-54.0	G	M	G	G	#6
KI0025F03:P9	3.5-50.5	B		B	B	#5, 7
KA3510A:P1	122.02-150					#?
KA3510A:P2	114.02-121.02	B		B	B	#15
KA3510A:P3	4.52-113.02	B			B	#3,4,5,6,8
KA3548A01:P1	15-30				B	#?
KA3548A01:P2	10-14				B	#?
KA3573A:P1	18-40				B	#15
KA3573A:P2	4.5-17				B	#5
KA3600F:P1	22-50.1	B		B	B	#?
KA3600F:P2	4.5-21	B		B	B	#5, 7?

INDEX 1=sp/Q
EXCELLENT
HIGH
MEDIUM
LOW
NO RESPONSE

INDEX 2=tr/R2
E=EXCELLENT
G=GOOD
M=MEDIUM
B=BAD

S=SINK

Figure 3-1. Pressure response matrix for tests A-1 to A-4.

3.3 Test A-1

The first test, A-1, performed by flowing section KI0025F03:P5 (structure #20), shows pressure responses (>1 kPa) in totally 45 borehole sections within the TRUE Block over distances ranging between 10 and 130 m. The flow rate was increased in two steps from 2.05 l/min to 2.70 l/min during the 67-hour flow period. The pump rate and the electrical conductivity versus time are shown in Figure 3-2. A summary of the flow rates used, drawdown and duration of the tests is shown in Table 3-1.

In the sink borehole, relatively large drawdown are also found in several sections adjacent to the sink section (KI0025F03:P4 and P6-P8), cf. Figure 3-1. This indicates that these sections, together with the sink section, are hydraulically connected to the same system of structures (#20-21, #23 and #6) as suggested by the structural (March'99) model. The response pattern indicates that the entire system of structures is (more or less) activated by this test.

The most significant drawdown responses are shown in Figure 3-3. Very good hydraulic responses occur in sections KA2563A:S4 (#20), KI0025F:R4 (#20), KI0023B:P7 (#6, 20), KI0025F02:P5 (#20), KI0023B:P6 (#21) and also in sections KI0025F02:P8 and KA2563A:S5, assumed to be intersected by #6. In addition, good but slightly more delayed responses occur in sections KI0023B:P5 (#18), KI0025F02:P6 (#22) and finally, in sections KA2563A:S3 (#13) and KI0023B:P4 (#13). The latter sections thus also appear to be (indirectly?) hydraulically connected to the same system of structures. The remainder of the responding sections show more delayed and attenuated responses.

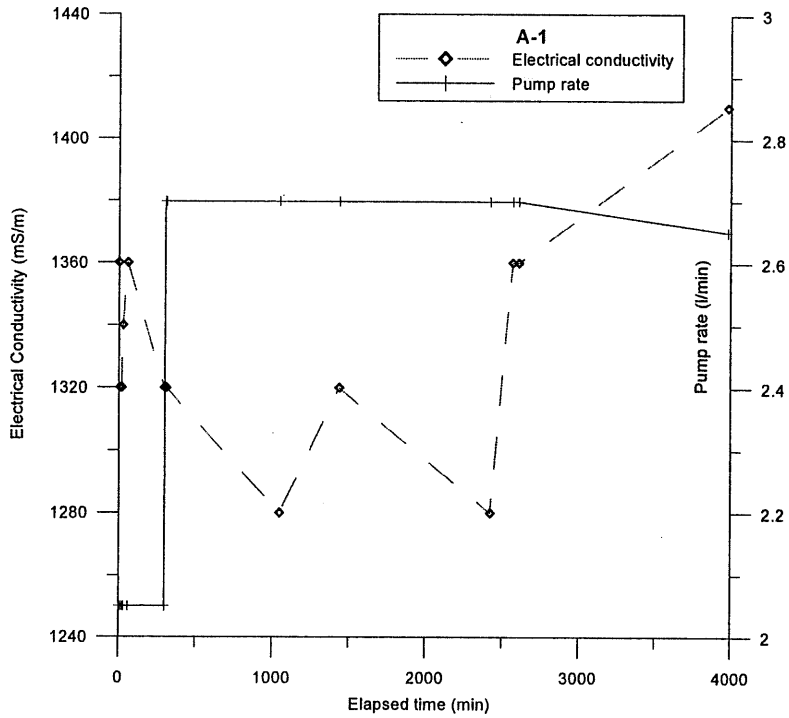

Figure 3-2. Pump rate and electrical conductivity of pumped water during test A-1.

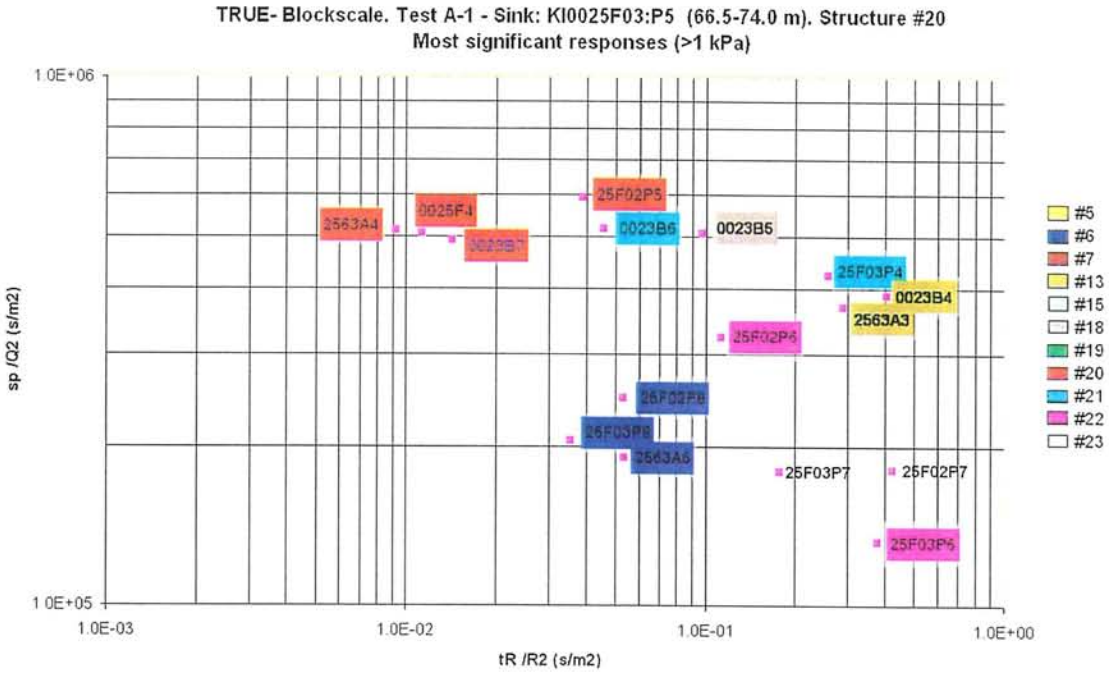

Figure 3-3. Pressure response plot showing the most significant responses during test A-1.

Test A-1 also included measurements of flow rates using the tracer dilution method in eighteen selected observation sections. The tests were performed both under natural gradient and during pumping in order to study the influence of the pumping. Test A-1 also included a 5-hour period with reduced pumping rate where in two sections also a flow rate has been possible to interpret from the dilution tests. The results presented in Table 3-2 show a distinct influence in 11 of the selected sections including structures #6, 13, 19, 20, 21 and 22, whereas 7 sections show a minor and/or uncertain change. In section KI0023B:P7 an extremely high flow (11 l/h) during natural conditions is observed as in the pre-tests (Andersson et al., 1999). This section contains a hydraulic short-circuit between structures #6 and #20 and the high flow is caused by the head difference between the structures. The flow direction is from #20 to #6, i.e towards the tunnel. Figure 3-4 shows a schematic plane view of borehole KI0023B and the intercepts with different structures. When pumping starts in the section containing structure #20, the gradient is reversed, or partly reversed, and the flow rate during pumping in KI0023B:P7 is decreased (0.4 l/h). Also in sections KA2563A:S1 and KI0025F02:P7 the flow rates were decreased as an effect of pumping. Section KI0023B:P6 (#21) shows strong pressure response but quite weak flow response. The flow responses in sections KI0025F02:P3 (#13, 21) and KI0025F03:P6 (#22) are very good while the pressure responses in these sections are weak.

Table 3-2. Results of tracer dilution tests during test A-1 using KI0025F03:P5 (#20) as sink. Q_{pump1} is for the 5-hour period of pumping with reduced flow rate, Q_{pump2} is for the period of pumping with maximum flow rate.

Test section	Structure	$Q_{natural}$ (ml/h)	Q_{pump1} (ml/h)	Q_{pump2} (ml/h)	ΔQ (ml/h)
KA2563A:S1	19	73		48	- 25
KA2563A:S3	13	4		9	+ 5
KA2563A:S4	20	199	511	604	+ 405
KI0025F:R4	20,22	6		9	+ 3
KI0023B:P2	19	20		19	- 1
KI0023B:P4	13	2		4	+ 2
KI0023B:P5	18	5		10	+ 5
KI0023B:P6	21	21		19	- 2
KI0023B:P7	6,20	11070		420	- 10650
KI0025F02:P3	13,21	46		143	+ 97
KI0025F02:P5	20	22		625	+ 603
KI0025F02:P6	22	270		728	+ 458
KI0025F02:P7	23	44		21	- 23
KI0025F02:P8	6	6		22	+ 16
KI0025F03:P3	13	17		16	- 1
KI0025F03:P4	21	16		15	- 1
KI0025F03:P6	22	64	307	378	+ 314
KI0025F03:P7	23	27		32	+ 5

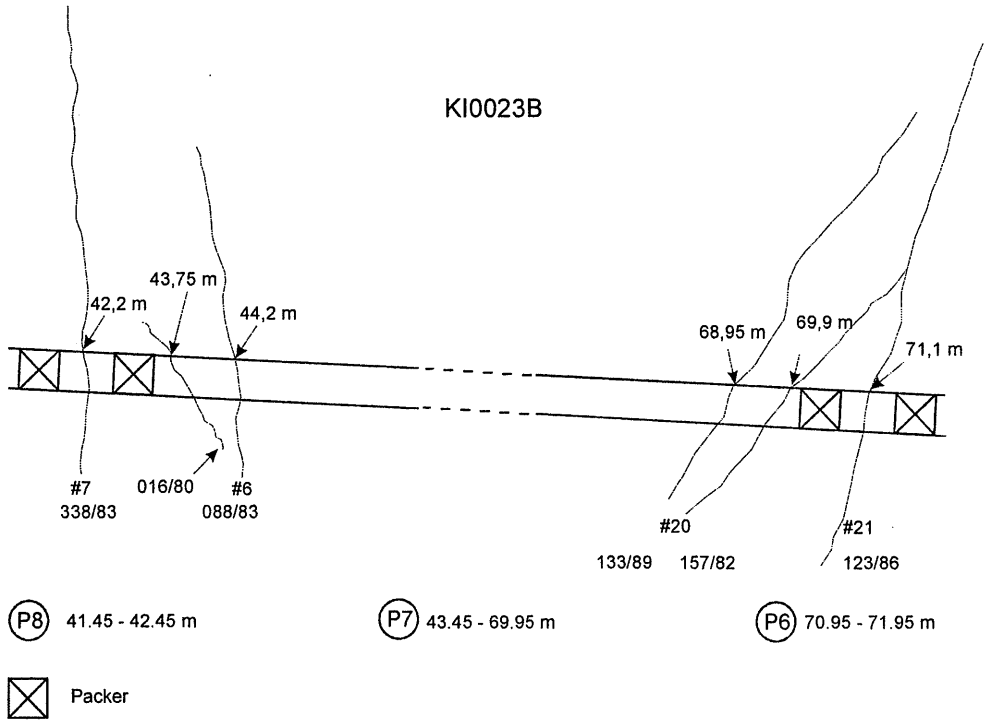

Figure 3-4. Schematic plane view of borehole KI0023B with fracture intersections in the packed-off sections P6, P7 and P8.

The most significant pressure response sections during A-1 are shown in a drawdown versus time/distance squared (t/R^2)-diagram in Figure 3-5. This type of transient response diagram provides similar information as the response diagram in Figure 3-3. The latter diagram shows the distribution of maximal drawdown at a fixed time, i.e. at stop of flowing, while the former shows the transient drawdown behaviour during the test. In a homogenous and isotropic medium all transient response curves should merge to a common curve.

Figure 3-5 shows that the tested rock is heterogeneous, despite that only the most significant responses are plotted. The calculated transmissivity and storativity from this analysis corresponds to the limiting Theis´-curve shown and thus mainly represent section KI0025F:R4. The Theis'-curve is matched to the first part of the response curves before the change of flow rate. All response curves show leaky (pseudo-spherical) flow by the end of the first flow rate step and steady-state flow by the end of the second step, c.f. the time-drawdown analysis.

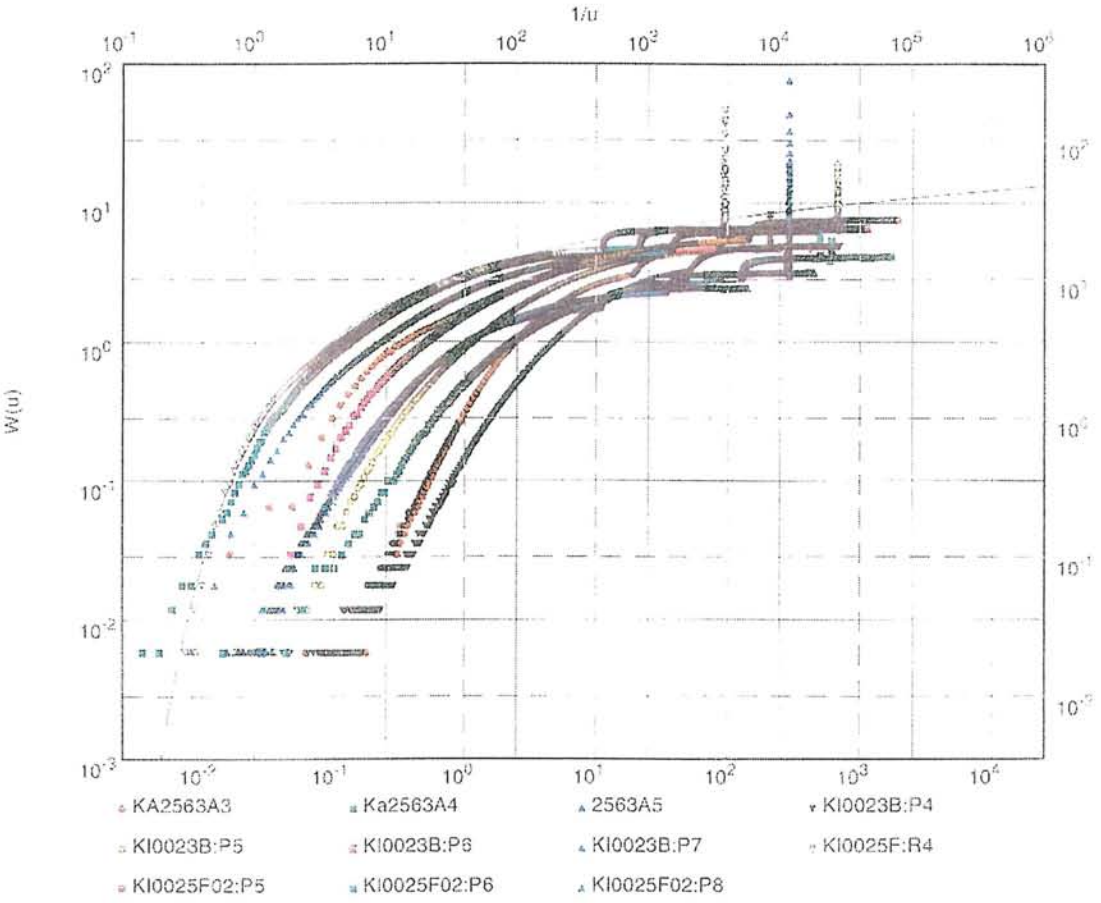

Figure 3-5. Drawdown versus t/R^2 diagram for test A-1. The line represents the Theis' curve for section KI0025F:R4. Evaluated parameters; T=7.6E-7 m^2/s, S=7.7E-8.

Quantitative (time-drawdown) evaluation is made on the sink section and on the most significant responses of the receiver sections according to the procedures described in Section 2.4.1. Only the first drawdown step has been analysed quantitatively. This is considered as sufficient for estimation of the hydraulic parameters. The transmissivity (T), storativity (S), the hydraulic diffusivity (T/S) and the leakage coefficient (K'/b') are estimated. In addition, the dominating flow geometry during the test and (apparent) hydraulic boundaries are deduced from the first step. The second step provides additional information on the ultimate flow geometry and potential hydraulic boundary conditions on a larger scale. The results for test A-1 are shown in Table 3-3.

The calculated values on the hydraulic parameters in the tables below represent parameters of an equivalent fractured porous medium. Accordingly, the interpretations of flow geometry and hydraulic boundaries also represent such a medium. The results from receiver sections within the sink borehole may be uncertain, e.g. due to non-radial flow between the sink and adjacent receiver sections.

The time-drawdown curves (including the drawdown derivative curves) of the sink section and of the most significant responses in the receiver sections exhibit a very similar flow geometry during the test. A short period of (pseudo)-radial flow geometry is transiting to leaky (pseudo-spherical) flow by the end of the the first drawdown step. Towards the end of the second step, a virtually steady-state flow occurred in all sections analysed. Only the effects of the tidal waves can be seen in the drawdown derivative curves.

The estimated values on transmissivity, storativity and hydraulic diffusivity for test A-1 are consistent with those estimated from other tests in the same structures, e.g. the Pre-tests (Andersson et al., 1999) and interference tests in KI0025F03 (Gentzschein and Ludvigson, 2000). The magnitude of the estimated values on the leakage coefficient K'/b' indicates only a slight leakance.

Table 3-3. Results of time-drawdown analysis for test A-1. S=Sink, Rad=Radial, Leaky=pseudospherical flow, SS=steady-state flow.

Borehole Section	Structure #	T (m^2/s)	S	T/S (m^2/s)	K'/b' (s^{-1})	Dom. Flow Geometry
KA2563A:S4	20	$7.6 \cdot 10^{-7}$	$9.6 \cdot 10^{-8}$	8.0	$9.1 \cdot 10^{-12}$	Leaky→SS
KI0025F:R4	20	$7.5 \cdot 10^{-7}$	$9.1 \cdot 10^{-8}$	8.2	$6.9 \cdot 10^{-12}$	Leaky→SS
KI0023B:P5	18	$6.8 \cdot 10^{-7}$	$8.2 \cdot 10^{-7}$	0.8	$6.9 \cdot 10^{-11}$	Leaky→SS
KI0023B:P6	21	$7.6 \cdot 10^{-7}$	$3.8 \cdot 10^{-7}$	2.0	$5.2 \cdot 10^{-11}$	Leaky→SS
KI0023B:P7	6, 20	$8.6 \cdot 10^{-7}$	$1.5 \cdot 10^{-7}$	5.7	$1.4 \cdot 10^{-11}$	Leaky→SS
KI0025F02:P5	20	$7.6 \cdot 10^{-7}$	$3.6 \cdot 10^{-7}$	2.1	$4.0 \cdot 10^{-11}$	Leaky→SS
KI0025F03:P5 (S)	20	$6.4 \cdot 10^{-7}$	-	-	-	Leaky→SS

3.4 Test A-2

Test A-2, performed by flowing section KI0025F03:P4 (structure #21), shows pressure responses (>1 kPa) in totally 18 receiver borehole sections within the TRUE Block over distances ranging between 4 and c. 50 m. The radius of influence (corresponding to a drawdown >1 kPa) is thus smaller for test A-2 than for A-1, possibly indicating less good hydraulic connection within the structure(s) tested. The flow rate was increased in two steps from 1.00 l/min to 1.18 l/min during the 71-hour flow period. A decrease in the electrical conductivity indicating increasing portion of less saline water was also noted (cf. Figure 3-6). A summary of the flow rates used, drawdown and duration of the tests is shown in Table 3-1.

In the sink borehole, relatively large drawdowns are found in several sections adjacent to the sink section (KI0025F03:P3 and P5-P8), cf. Figure 3-1. This indicates that these sections, together with the sink section, are hydraulically connected to the same system of structures (#20-21, #23, #6 and #13) as suggested by the Structural (March'99) model.

The most significant drawdown responses are shown in Figure 3-7. This figure shows that the (normalised) response times of the most significant responses are longer for test A-2 compared to A-1, again indicating decreased hydraulic connection within the structure tested. Relatively good hydraulic responses occur in sections KA2563A:S4 (#20), KI0023B:P7 (#6, 20), KI0023B:P6 (#21), KI0025F:R4 (#20) and in sections KI0025F02:P8 and KA2563A:S5, assumed to be intersected by #6.

Strong, but delayed responses occur in sections KI0023B:P5 (#18), KI0025F02:P5 (#20), KI0025F02:P6 (#22) and finally, in sections KA2563A:S3 (#13) and KI0023B:P4 (#13). The latter sections thus also appear to be hydraulically connected to the tested system of structures. The remainder of the responding sections in the receiver boreholes shows even more delayed responses.

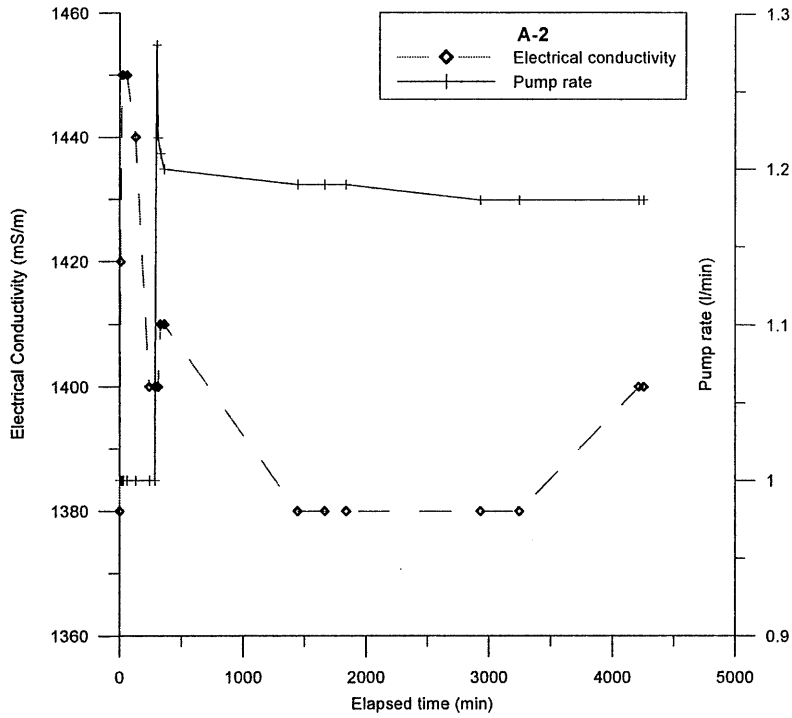

Figure 3-6. Pump rate and electrical conductivity of pumped water during test A-2.

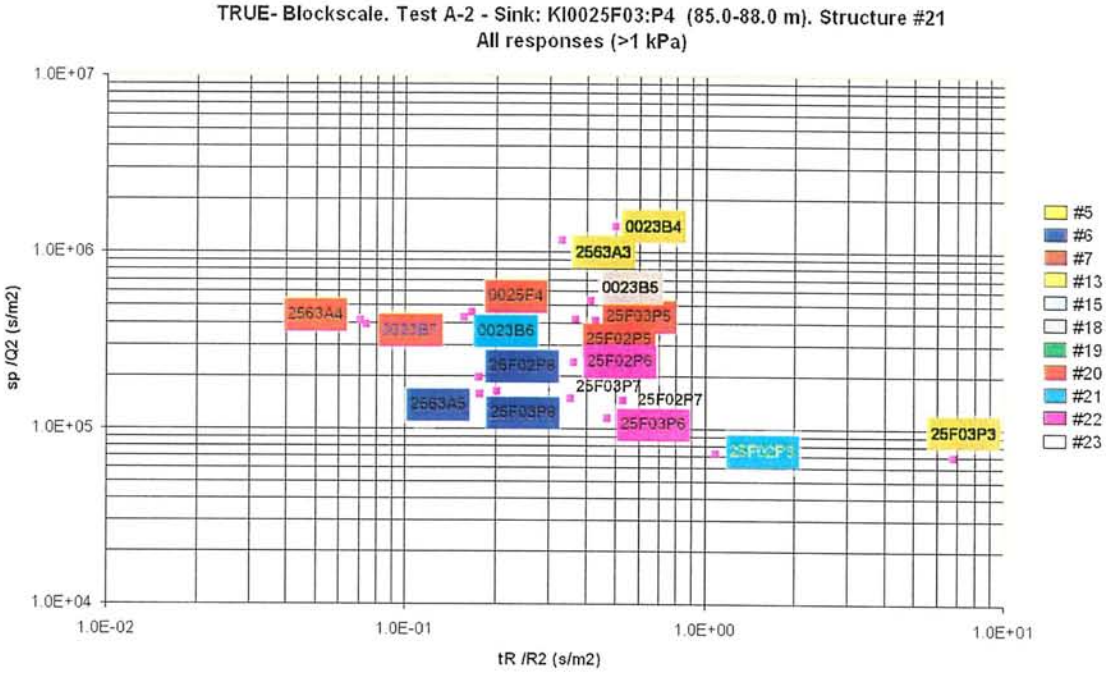

Figure 3-7. Pressure response plot showing the drawdown responses during test A-2.

Test A-2 included measurements of flow rates using the tracer dilution method in eighteen selected observation sections. The tests were performed both under natural gradient and during pumping in order to study the influence of the pumping. Test A-2 also included a 5-hour period with reduced pumping rate where in one section also a flow rate has been possible to interpret from the dilution tests.The results presented in Table 3-4 show a distinct influence in 10 of the selected sections, including structures # 6, 13, 19, 20, 21 and 22 whereas 7 sections have a minor and/or uncertain increase/decrease and one section (KI0025F02:P7) shows no change at all. The flow in section KA2563A:S4 (#20) was decreased by half when pumping started. This section together with section KI0023B:P7 are those showing the best pressure responses in test A-2. Also in test A-2 a high "natural" flow (11 l/h) in section KI0023B:P7 was observed which was decreased when pumping started in structure #21. This is caused by the hydraulic short-circuit in the section, cf. Figure 3-4, and is further discussed in Section 3.3. Sections KA2563A:S1 (#19), KI0025F02:P3 (#13, 21) and KI0025F03:P6 (#22) show strong flow responses while the pressure responses are weak.

Table 3-4. Results of tracer dilution tests during test A-2 using KI0025F03:P4 (#21) as sink. Q_{pump1} is for the five-hour period of pumping with reduced flow rate, Q_{pump2} is for the period of pumping with maximum flow rate.

Test section	Structure	$Q_{natural}$ (ml/h)	Q_{pump1} (ml/h)	Q_{pump2} (ml/h)	ΔQ (ml/h)
KA2563A:S1	19	21		87	+ 66
KA2563A:S3	13	5		9	+ 4
KA2563A:S4	20	201		100	- 101
KI0025F:R4	20,22	2		3	+ 1
KI0023B:P2	19	16		13	- 3
KI0023B:P4	13	5		8	+ 3
KI0023B:P5	18	5		120	+ 115
KI0023B:P6	21	4		13	+ 9
KI0023B:P7	6,20	11030		677	- 10353
KI0025F02:P3	13,21	25		562	+ 537
KI0025F02:P5	20	11		21	+ 10
KI0025F02:P6	22	138		485	+ 347
KI0025F02:P7	23	10		10	± 0
KI0025F02:P8	6	8		9	+ 1
KI0025F03:P3	13	9		15	+ 6
KI0025F03:P5	20	0		5	+ 5
KI0025F03:P6	22	78	162	196	+ 118
KI0025F03:P7	23	22		23	+ 1

As for test A-1, the most significant pressure response during test A-2 are shown in a drawdown versus time/distance squared (t/R^2)-plot in Figure 3-8. The plot shows that the tested medium is heterogeneous, despite that only the most significant responses are plotted. The strong but more delayed responses in sections KA2563A:S3 and

KI0023B:P4, both assumed to be located in #13, are clearly seen. All responses are more delayed compared to test A-1, c.f. Figure 3-7 and associated discussion.

The calculated transmissivity and storativity shown in Figure 3-8 corresponds to the limiting Theis´-curve shown and thus mainly represent section KA2563A:S4. The Theis'-curve is matched to the first part of the response curves before the change of flow rate. As for test A-1, all response curves show leaky (pseudo-spherical) flow by the end of the first flow rate step and virtually steady-state flow by the end of the second step, c.f. the time-drawdown analysis below.

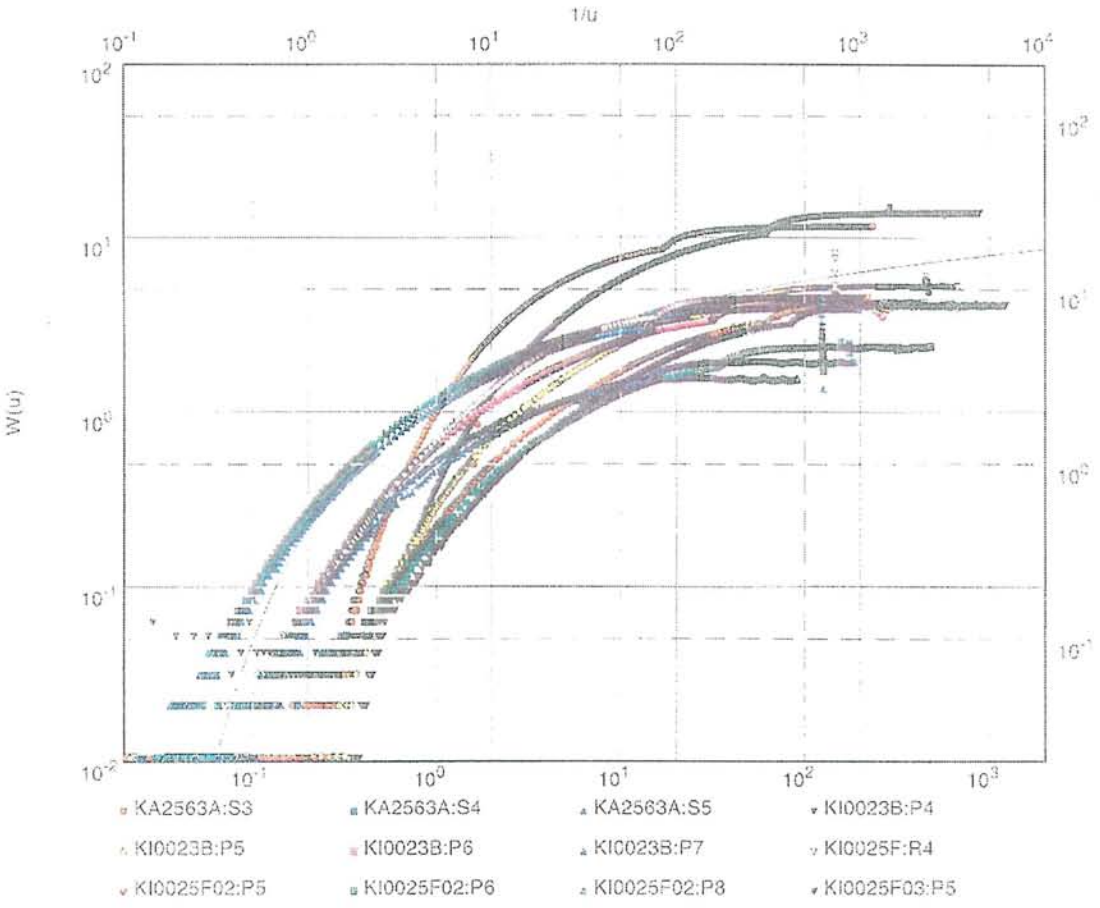

Figure 3-8. Drawdown versus t/R^2 diagram for test A-2. The line represents the Theis' curve for section KA2563A:S4. Evaluated parameters; T=6.7E-7 m^2/s, S=5.3E-7.

The estimated hydraulic parameters for test A-2, as described in section 2.4.1, are shown in Table 3-5.

The time-drawdown curves (including the drawdown derivative curves) of the sink section and of the most significant responses in the receiver sections exhibit a very similar flow geometry during the test. A short period of (pseudo)-radial flow geometry is transiting to leaky (pseudo-spherical) flow by the end of the the first drawdown step.

Towards the end of the second step, a virtually steady-state flow occurred in all sections analysed. Only the effects of the tidal waves can be seen in the drawdown derivative curves.

The estimated transmissivities are generally in the same order as for test A-1, whereas the storativities in general are about 5-10 times higher. This implies that the hydraulic diffusivities are c. 5-10 times lower, which is consistent with the slower response times as discussed above. The values on the leakage coefficient are slightly higher for test A-2 compared to A-1.

Table 3-5. Results of time-drawdown analysis for test A-2. S=Sink, Rad=Radial, Leaky=pseudospherical (>2D) flow, SS=steady-state flow.

Borehole Section	Structure #	T (m^2/s)	S	T/S (m^2/s)	K'/b' (s^{-1})	Dom. Flow Geometry
KA2563A:S3	13	$2.1 \cdot 10^{-7}$	$4.1 \cdot 10^{-7}$	0.5	$2.6 \cdot 10^{-11}$	Leaky→SS
KA2563A:S4	20	$7.4 \cdot 10^{-7}$	$4.6 \cdot 10^{-7}$	1.6	$1.2 \cdot 10^{-11}$	Leaky→SS
KI0025F:R4	20	$5.2 \cdot 10^{-7}$	$8.6 \cdot 10^{-7}$	0.6	$2.8 \cdot 10^{-11}$	Leaky→SS
KI0023B:P4	13	$2.0 \cdot 10^{-7}$	$8.2 \cdot 10^{-7}$	0.2	$3.9 \cdot 10^{-11}$	Leaky→SS
KI0023B:P6	21	$7.3 \cdot 10^{-7}$	$1.1 \cdot 10^{-6}$	0.7	$1.3 \cdot 10^{-11}$	Leaky→SS
KI0023B:P7	6, 20	$7.8 \cdot 10^{-7}$	$5.2 \cdot 10^{-7}$	1.5	$1.1 \cdot 10^{-11}$	Leaky→SS
KI0025F03:P4 (S)	21	$3.0 \cdot 10^{-8}$	-	-	-	Leaky→SS

3.5 Test A-3

Test A-3, performed by flowing section KI0025F02:P5 (structure #20), shows pressure responses (>1 kPa) in totally 41 receiver borehole sections within the TRUE Block over distances ranging between c. 10 m and c. 130 m. The drawdown pattern is very similar to that for test A-1. The flow rate was increased from 3.60 l/min to 4.10 l/min during the 46-hour pumping period. A decrease in the electrical conductivity indicating increasing portion of less saline water was also noted (cf. Figure 3-9). A summary of the flow rates used, drawdown and duration of the tests is shown in Table 3-1.

In the sink borehole, relatively large drawdowns are found in several sections adjacent to the sink section (KI0025F02:P3 and P6-P8), cf. Figure 3-1. This indicates that these sections, together with the sink section, are hydraulically connected to the same system of structures (#20, #21, #22, #6 and #13) as suggested by the Structural (March'99)

model. The response pattern in the sink borehole indicates that the entire system of structures is (more or less) activated in this borehole during the test.

The most significant drawdown responses during test A-3 are shown in Figure 3-10. The response pattern is very similar to that during test A-1, performed in the same structure and also to that for Pre-Test #3 (except borehole KFI0025F03) with the same sink section (Andersson et al., 1999). The figure shows that the (normalised) response times of the most significant responses are quite short, indicating good hydraulic connection (high hydraulic diffusivity) within the structure tested. Very good responses occur in sections KA2563A:S4 (#20), KI0023B:P7 (#6, 20), KI0025F03:P5 (#20) , KI0025F:R4 (#20) and KI0023B:P6 (#21). Good responses also occur in sections KA2563A:S5, KI0025F02:P8 and KI0025F03:P8, assumed to be intersected by #6.

Strong, but more delayed responses occur in sections KI0023B:P5 (#18), KI0025F03:P4 (#21) and KI0025F02:P6 (#22) and finally, in sections KA2563A:S3 (#13) and KI0023B:P4 (#13). The latter sections thus also appear to be (indirectly?) hydraulically connected to the tested system of structures. The remainder of the responding sections show more delayed and attenuated responses.

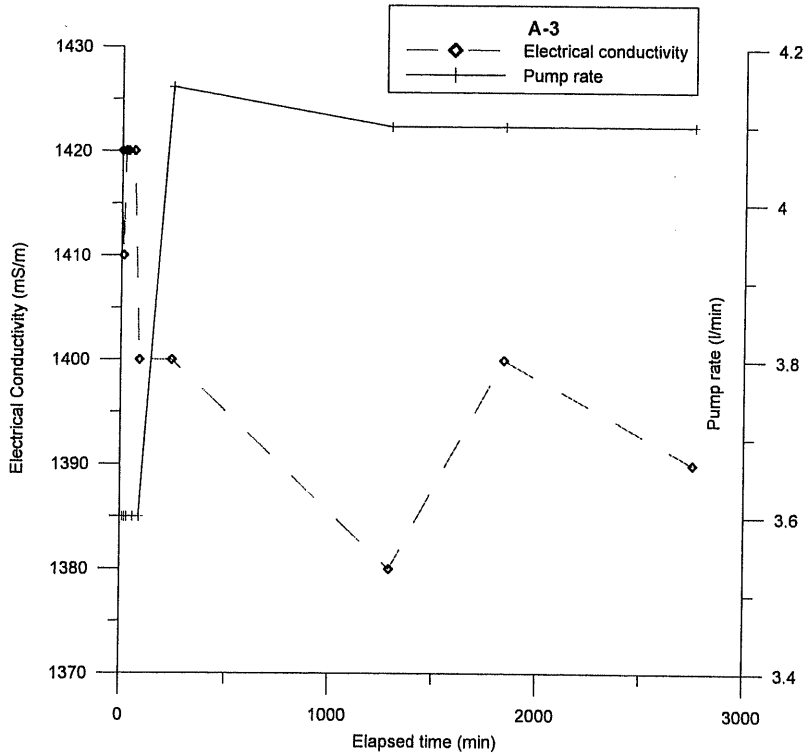

Figure 3-9. Pump rate and electrical conductivity of pumped water during test A-3.

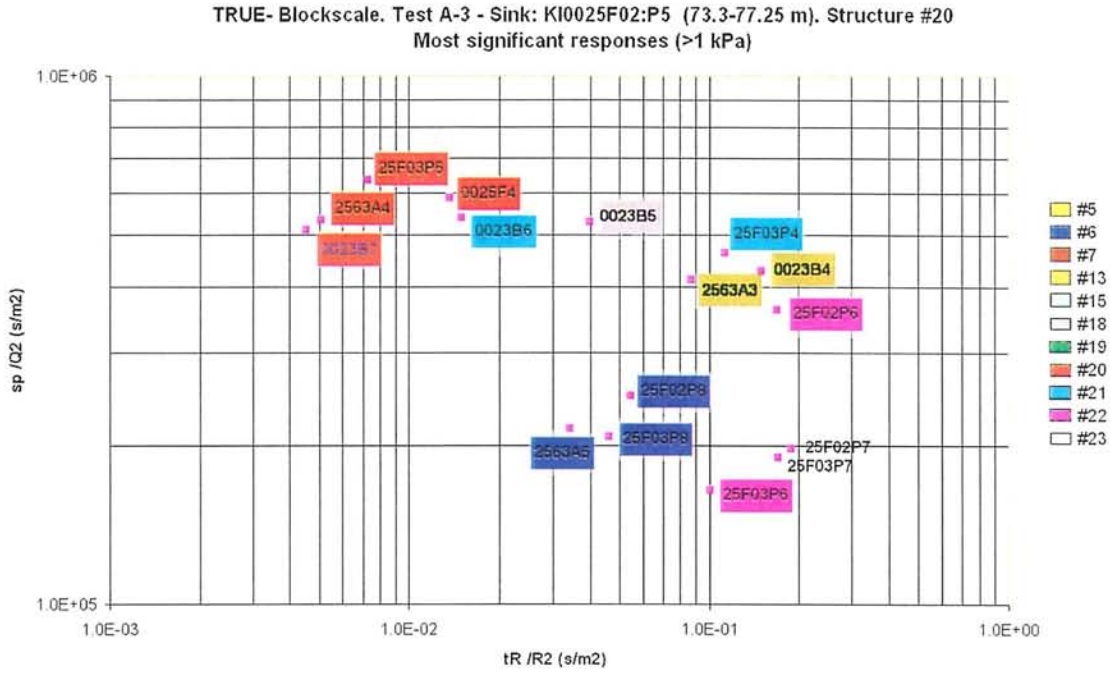

Figure 3-10. Pressure response plot showing the most significant responses during test A-3.

A-3 included measurements of flow rates using the tracer dilution method in twelve selected observation sections. The test were performed both under natural gradient and during pumping in order to study the influence of the pumping. Test A-3 also included a 4-hour period with reduced pumping rate but no influence of the flow in the tested sections, different from the one recieved when pumping with maximum flow, could be interpreted from the dilution tests. The results presented in Table 3-6 show a distinct influence in 8 of the selected sections containing structures #6, 13, 20, 21 and 22 whereas 3 sections show a minor and/or uncertain increase and one section (KI0025F02:P7) shows no change at all. In section KA2563A:S3 (#13) the flow decreased from 10 ml/h during "unpumped" conditions to 0 ml/h during pumping. Also in test A-3 a high "natural" flow (11 l/h) in section KI0023B:P7 was observed which was decreased when pumping started in structure #20. This is caused by the hydraulic short-circuit in the section, cf. Figure 3-4, and is further discussed in Section 3.3. The flow responses in sections KI0025F02:P3 and KI0025F03:P6 are very good while the pressure responses are weak.

Table 3-6. Results of tracer dilution tests during test A-3 using KI0025F02:P5 (#20) as sink. Q_{pump1} is for the five-hour period of pumping with reduced flow rate, Q_{pump2} is for the period of pumping with maximum flow rate.

Test section	Structure	$Q_{natural}$ (ml/h)	Q_{pump1} (ml/h)	Q_{pump2} (ml/h)	ΔQ (ml/h)
KA2563A:S3	13	10		0	- 10
KI0025F:R4	20,22	3		6	+ 3
KI0023B:P4	13	4		6	+ 2
KI0023B:P5	18	5		11	+ 6
KI0023B:P7	6,20	11550		350	- 11200
KI0025F02:P3	13,21	30		205	+ 175
KI0025F02:P7	23	9		9	± 0
KI0025F03:P3	13	0		6	+ 6
KI0025F03:P4	21	6		14	+ 8
KI0025F03:P5	20	5		36	+ 31
KI0025F03:P6	22	75		685	+ 610
KI0025F03:P7	23	25		28	+ 3

The most significant pressure response sections during test A-3 are shown in a drawdown versus time/distance squared (t/R^2)-plot in Figure 3-11. The plot shows that the tested medium is heterogeneous, despite that only the most significant responses are plotted. Again, the plot is very similar to that for test A-1.

The calculated transmissivity and storativity shown in the plot corresponds to the limiting Theis´-curve shown and thus mainly represent section KA2563A:S4. The Theis'-curve is matched to the first part of the response curves before the change of flow rate. As for the previous tests, all response curves show leaky (pseudo-spherical) flow by the end of the first flow rate step and virtually steady-state flow by the end of the second step, c.f. the time-drawdown analysis below.

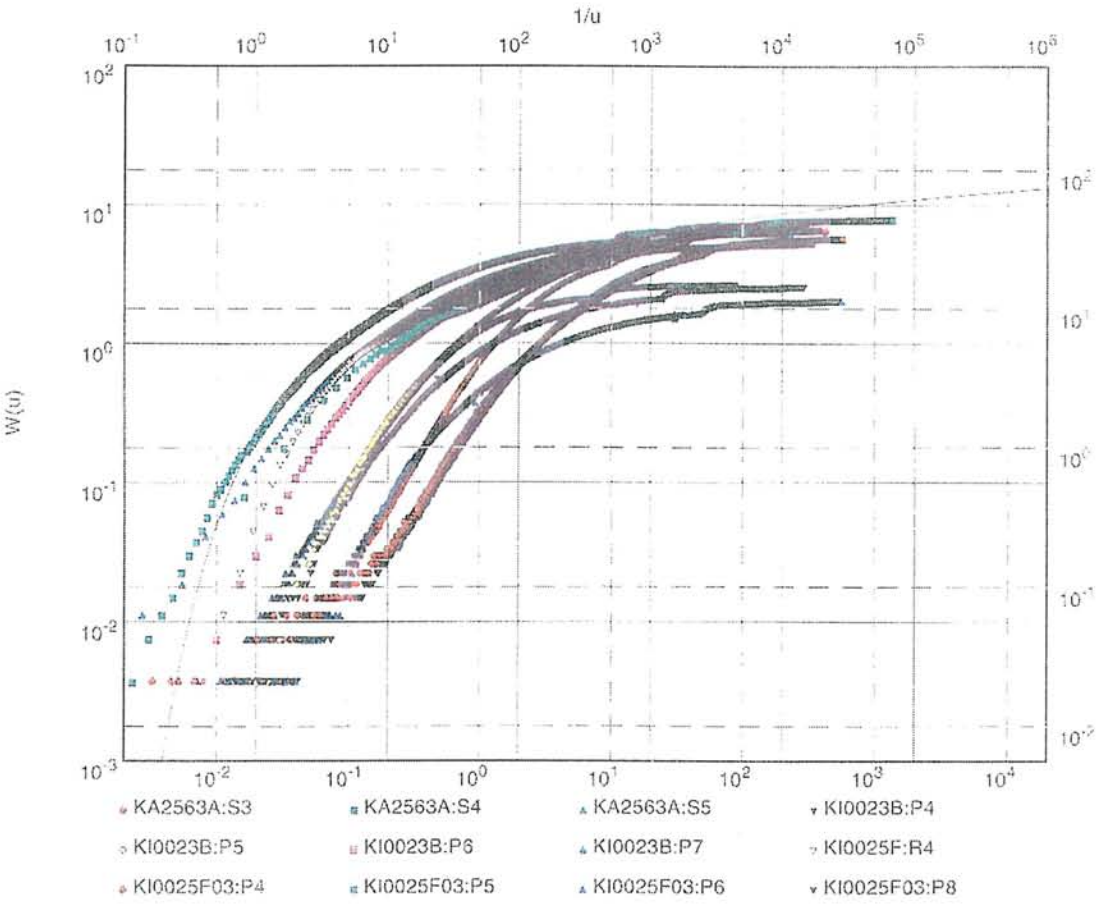

Figure 3-11. Drawdown versus t/R^2 diagram for test A-3. The line represents the Theis' curve for section KA2563A:S4. Evaluated parameters; T=8.5E-7 m^2/s, S=6.8E-8.

The estimated hydraulic parameters for test A-3, as described in section 2.4.1, are shown in Table 3-7.

The time-drawdown curves (including the drawdown derivative curves) of the sink section and of the most significant responses in the receiver sections exhibit a very similar flow geometry during the test. A short period of (pseudo)-radial flow geometry is transiting to leaky (pseudo-spherical) flow by the end of the the first drawdown step. Towards the end of the second step, a virtually steady-state flow (or possible, a very minor decreasing pressure trend) occurred in all sections analysed. The effects of the tidal waves dominate the drawdown derivative curves by the end of the test. This is not in agreement with the observed pressure trend by the end of Pre-Test #3 which indicated a no-flow boundary. However, the duration of the latter test was about two times longer (93 h), which may explain this behaviour.

The estimated values on transmissivity, storativity and hydraulic diffusivity for test A-3 are consistent with those estimated from test A-1 and other tests in the same structures, e.g. the Pre-tests (Andersson et al., 1999) and interference tests in KI0025F03

(Gentzschein and Ludvigson, 2000). The magnitude of the estimated values on the leakage coefficient K'/b' indicates only a slight leakance.

Table 3-7. Results of time-drawdown analysis for test A-3. S=Sink, Rad=Radial, Leaky=pseudospherical (>2D) flow, SS=steady-state flow.

Borehole Section	Structure #	T (m^2/s)	S	T/S (m^2/s)	K'/b' (s^{-1})	Dom. Flow Geometry
KA2563A:S4	20	$7.6 \cdot 10^{-7}$	$7.2 \cdot 10^{-8}$	10.6	$8.9 \cdot 10^{-12}$	Leaky→SS
KI0025F:R4	20	$6.9 \cdot 10^{-7}$	$2.2 \cdot 10^{-7}$	3.1	$1.3 \cdot 10^{-11}$	Leaky→SS
KI0023B:P6	21	$7.3 \cdot 10^{-7}$	$2.4 \cdot 10^{-7}$	3.0	$1.5 \cdot 10^{-11}$	Leaky→SS
KI0023B:P7	6, 20	$8.1 \cdot 10^{-7}$	$1.3 \cdot 10^{-7}$	6.4	$1.3 \cdot 10^{-11}$	Leaky→SS
KI0025F02:P5 (S)	20	$7.5 \cdot 10^{-7}$	-	-	-	Leaky→SS
KI0025F03:P5	20	$7.4 \cdot 10^{-7}$	$3.7 \cdot 10^{-7}$	2.0	$2.2 \cdot 10^{-11}$	Leaky→SS

3.6 Test A-4

3.6.1 Interference tests and dilution tests

Test A-4, performed by flowing section KI0023B:P6 (structure #21), shows pressure responses (>1 kPa) in totally 52 receiver borehole sections within the TRUE Block over distances ranging between c. 10 m and c. 130 m. The flow rate was increased from 2.05 l/min to 2.30 l/min during the long-term (24 days) flow period. The drawdown pattern is very similar to that for tests A-1 and A-3. An increase in the electrical conductivity indicating increasing portion of more saline water was also noted (cf. Figure 3-12). A summary of the flow rates used, drawdown and duration of the tests is shown in Table 3-1.

In the sink borehole, relatively large drawdowns are found in adjacent sections to the sink (KI0023B:P7 and P4-P5), cf. Figure 3-1. This indicates that these sections, together with the sink section, are hydraulically connected to the same system of structures (#20-21, #6 and #13 and #18) as suggested by the Structural (March'99) model. The response pattern in the sink borehole indicates that the entire system of structures is (more or less) activated in this borehole during the test.

The most significant drawdown responses during test A-4 are shown in Figure 3-13. The response pattern is very similar to that during tests A-1 and A-3, performed in structure #20. The response pattern is also similar to that for the older interference test

in KI0023B:P6 (except borehole KFI0025F03), reported in Andersson et al, 1998. However, during test A-4 section KI0023B:P5, adjacent to the sink section, responded almost instantaneously but the drawdown then decreased to increase again (pressure wave).

Figure 3-13 shows that the (normalised) response times of the most significant responses are quite short, indicating good hydraulic connection (high hydraulic diffusivity) within the structure tested. Very good responses occur in sections KA2563A:S4 (#20), KI0023B:P7 (#6, 20), KI0025F03:P5 (#20) , KI0025F:R4 (#20) and KI0025F02:P5 (#20). This indicates that the sink section (KI0023B:P6) may be located in structure #20 instead of #21, assumed in the structural model. Good responses also occur in section KI0023F03:P4 (#21) and in sections KA2563A:S5, KI0025F02:P8 and KI0025F03:P8, all assumed to be intersected by #6.

Strong, but more delayed responses occur in sections KI0025F02:P6 and KI0025F03:P6, both in structure #22 and finally, in sections KA2563A:S3 and KI0023B:P4, both in structure #13. The latter sections thus also appear to be (indirectly?) hydraulically connected to the tested system of structures. The remainder of the responding sections show more delayed and attenuated responses.

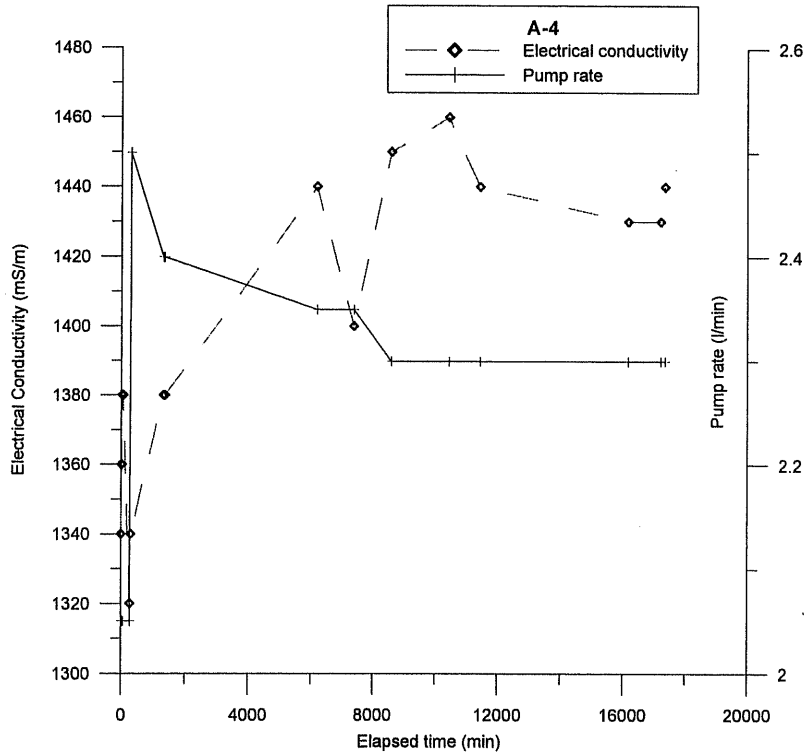

Figure 3-12. Pump rate and electrical conductivity of pumped water during test A-4.

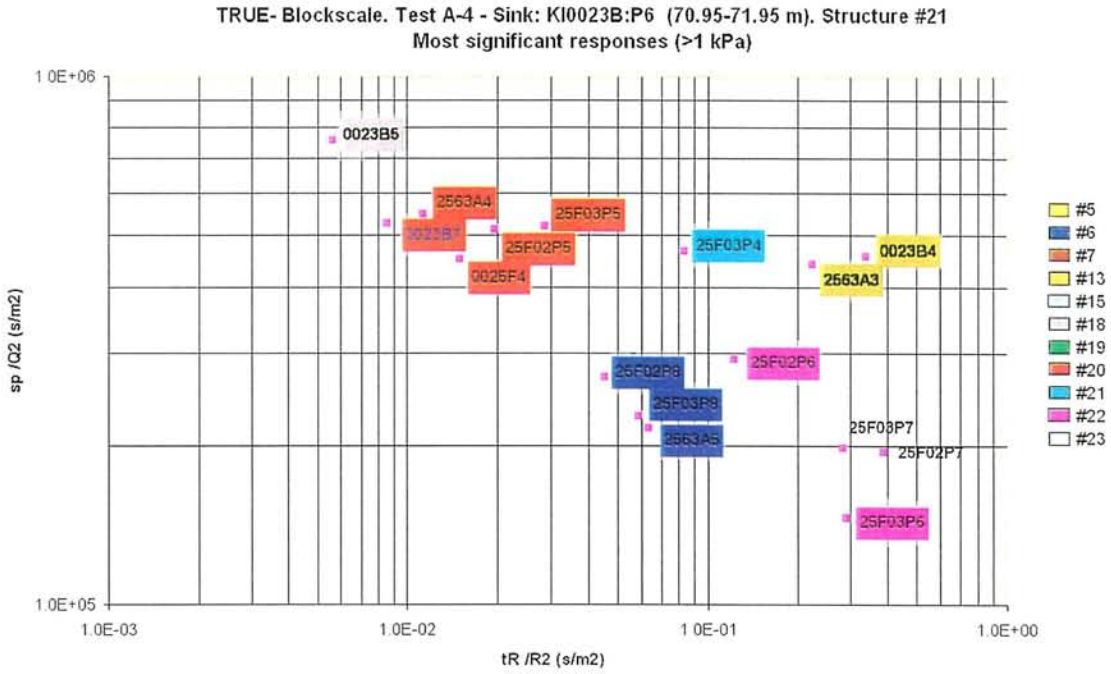

Figure 3-13. Pressure response plot showing the most significant responses during test A-4.

A-4 included measurements of flow rates using the tracer dilution method in five selected observation sections. The test were performed both under natural gradient and during pumping in order to study the influence of the pumping. Test A-4 also included a 5-hour period with reduced pumping rate but no influence of the flow in the tested sections, different from the one recieved when pumping with maximum flow, could be interpreted from the dilution tests. The results presented in Table 3-8 show a distinct influence in 3 of the selected sections containing structures #20, 21 and 22 whereas 2 sections show a minor and/or uncertain increase. The flow response in section KI0025F03:P6 is very good while the pressure response is weak.

Table 3-8. Results of tracer dilution tests during test A-4 using KI0023B:P6 (#21) as sink. Q_{pump1} is for the five-hour period of pumping with reduced flow rate, Q_{pump2} is for the period of pumping with maximum flow rate.

Test section	Structure	$Q_{natural}$ (ml/h)	Q_{pump1} (ml/h)	Q_{pump2} (ml/h)	ΔQ (ml/h)
KI0025F03:P3	13	4		10	+ 6
KI0025F03:P4	21	1		10	+ 9
KI0025F03:P5	20	2		35	+ 33
KI0025F03:P6	22	90		410	+ 320
KI0025F03:P7	23	32		39	+ 7

The most significant pressure response sections (including the tracer dilution sections) during test A-4 are shown in a drawdown versus time/distance squared (t/R^2)-plot in Figure 3-14. The plot shows that the tested medium is heterogeneous, despite that only the most significant responses are plotted. Again, the plot is very similar to that for tests A-1 and A-3.

The calculated transmissivity and storativity shown in the plot corresponds to the limiting Theis´-curve shown and thus mainly represent section KI0025F:R4. The Theis'-curve is matched to the first part of the response curves before the change of flow rate. As for the previous tests, all response curves show leaky (pseudo-spherical) flow by the end of the first flow rate step and virtually steady-state flow by the end of the second step, c.f. the time-drawdown analysis below.

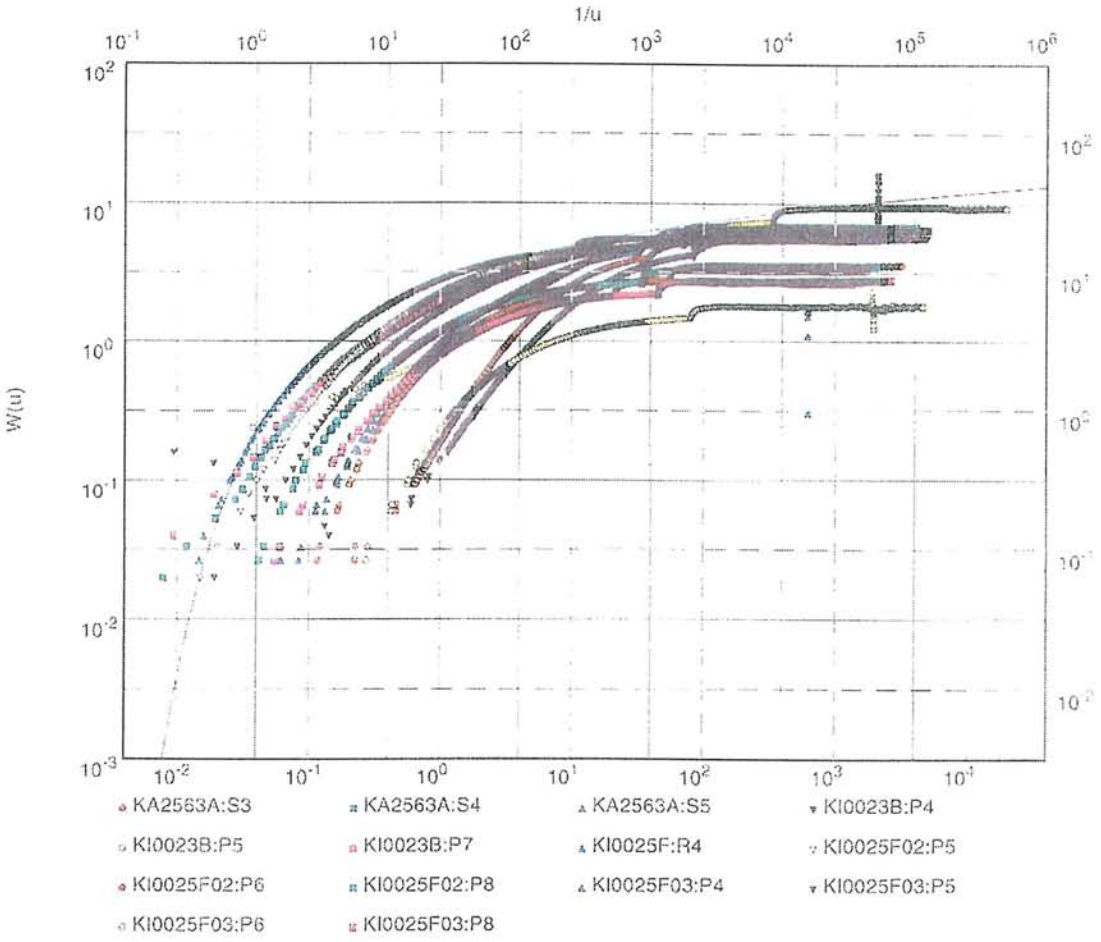

Figure 3-14. Drawdown versus t/R^2 diagram for test A-4. The line represents the Theis' curve for section KI0025F:R4. Evaluated parameters; T=8.6E-7 m^2/s, S=1.4E-7.

The estimated hydraulic parameters for test A-4, as described in section 2.4.1, are shown in Table 3-9.

The time-drawdown curves (including the drawdown derivative curves) of the sink section and of the most significant responses in the receiver sections exhibit a very similar flow geometry during the test. A short period of (pseudo)-radial flow geometry is transiting to leaky (pseudo-spherical) flow by the end of the the first drawdown step. Towards the end of the second step, a virtually steady-state flow (or possible, a very minor decreasing pressure trend) occurred in all sections analysed. The effects of the tidal waves dominate the drawdown derivative curves by the end of the test. This is in agreement with the observed pressure trend by the end of the old interference test in KI0023B:P6, although the latter test had a much shorter duration (24 h). The latter test also indicated the presence of a constant-head boundary by the end of the test (Andersson & Ludvigson, 1999).

The estimated values on transmissivity, storativity and hydraulic diffusivity for test A-4 are consistent with those estimated from tests A-1 and A-3. The magnitude of the estimated values on the leakage coefficient K'/b' are though slightly higher.

Table 3-9. Results of selective time-drawdown analysis for test A-4. S=Sink, Rad=Radial, Leaky=pseudospherical (>2D) flow, SS=steady-state flow.

Borehole Section	Structure #	T (m^2/s)	S	T/S (m^2/s)	K'/b' (s^{-1})	Dom. Flow Geometry
KI0023B:P6 (S)	21	$5.4 \cdot 10^{-7}$	-	-	-	Leaky→SS
KI0025F03:P4	21	$7.6 \cdot 10^{-7}$	$8.3 \cdot 10^{-7}$	0.9	$3.3 \cdot 10^{-11}$	Leaky→SS
KI0025F03:P5	20	$7.9 \cdot 10^{-7}$	$4.1 \cdot 10^{-7}$	1.9	$5.2 \cdot 10^{-11}$	Leaky→SS
KI0025F03:P8	6	$1.5 \cdot 10^{-6}$	$8.4 \cdot 10^{-7}$	1.8	$5.7 \cdot 10^{-10}$	Leaky→SS

3.6.2 Tracer test

Test A-4 also involved a cross-hole tracer test, using KI0023B:P6 as sink. Based on the results from the earlier performed dilution tests in A-4 three sections were chosen for injections, KI0025F03:P5, KI0025F03:P6 and KI0025F03:P7. Pumping was done in KI0023B:P6 (structure #21) using maximum possible flow, 2.3 l/min.

Tracer injections

The injections were performed as decaying pulses. In one injection (section KI0025F03:P5), the tracer solution was exchanged with non-traced water in order to shorten the tail of the breakthrough curve. The removal of tracer resulted in a reduction of about 90 % of the mass in the tracer injection loop. The injection concentrations and injection rates are given in Table 3-10 and are the actually measured ones.

The injected mass was both weighed using a scale and calculated by integration of the injection concentration versus time. There is a discrepancy between the two numbers that, at least partly, can be explained by the fact that a large portion of the mass still remains in the injection section at the time when smapling was finished (165 hours).

Table 3-10. Tracer injection data for test A-4 (measured values).

Inj #	Section	Structure #	Tracer	Max inj. conc (mg/l)	Inj rate (ml/h)*	Inj mass (mg)	Section Volume (ml)
1	KI0025F03:P6	22	Amino-G Acid	595	341	3248[1] 4223[2]	5687
2	KI0025F03:P7	23	Rhodamine WT	105	27	284[1] 902[2]	4978
3	KI0025F03:P5	20	Uranine	150	31	132 -	7214

*Calculated from the tracer dilution during injection
[1]=calculated by integration
[2]=calculated by weighing

The injection functions presented as the logarithm of concentration (Ln C) versus time are shown in Figure 3-15.

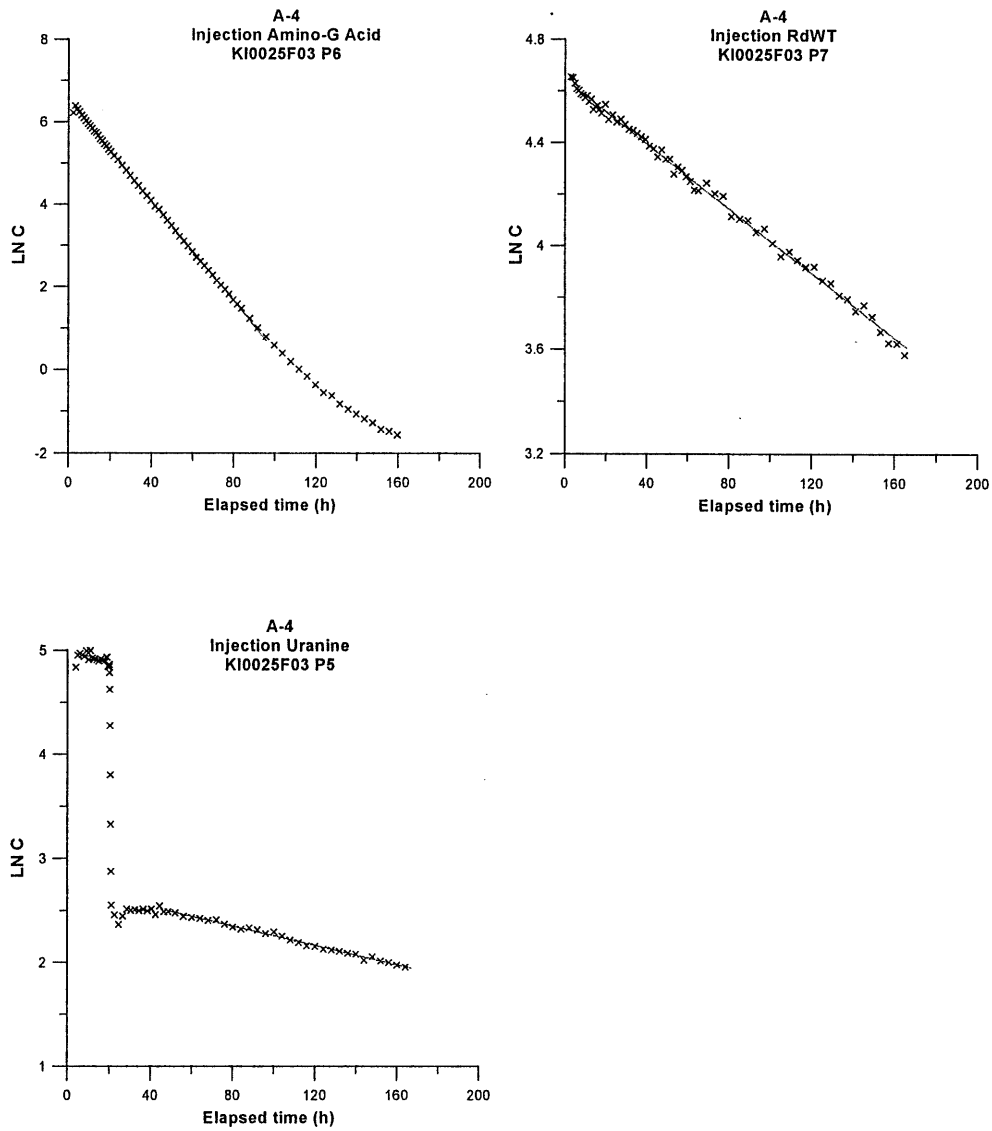

Figure 3-15. Tracer injection functions (Ln C versus time) including straight-line fits for the three injections during test A-4. Note that the axis scales differ.

Tracer breakthrough

Tracer breakthrough was detected in the sink section KI0023B:P6 from two of the three injections performed and the resulting breakthrough curves are presented in Figure 3-16. The breakthrough and injection curves are also plotted together (as mass flux versus time, log-log) in the same plot in Appendix 1. No breakthrough from the injection of Rhodamine WT in section KI0025F03:P7 was detected at pump stop after 165 hours.

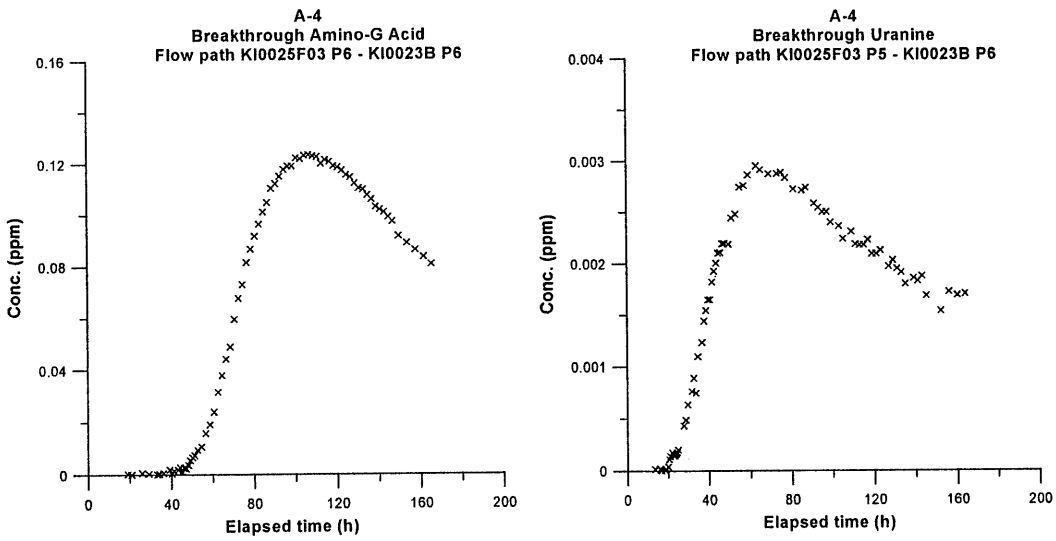

Figure 3-16. Tracer breakthrough in KI0023B:P6 during test A-4. Note that the axis scales differ between the plots.

The pumping was stopped on November 30th, 1999 after a pumping period of 12 days. No major equipment failure occurred during the test period.

Tracer mass recovery was for Amino-G Acid calculated in two different ways. Common for both methods was that the tracer mass recovered in the pumping borehole was determined by integration of the breakthrough curves for mass flux (mg/h) versus time (h). The injected mass was determined in the same way but also by weighing the tracer solution vessel during the injection procedure. In injection section KI0025F03:P5 (Uranine) a tracer exchange procedure was made. Unfortunately no samples were taken of the tracer solution exchanged why it is not possible to calculate the injected mass by weighing. The calculated injected masses are shown in Table 3-10.

The mass recovery for Amino-G Acid calculated from integration is higher than the one calculated by weighing (Table 3-11). The reason for this is further discussed in Section 3.7.2. A large portion of the tail of the breakthrough curves still remains to be recovered, and it is therefore likely that the mass recovery would have increased by another 20-30 %.

Table 3-11. Tracer mass recoveries from pumping section KI0023B:P6 during test A-4.

Inj #	Section	Structure	Tracer	R_i (%)	R_w (%)	Sampling time (h)
1	KI0025F03:P6	22	Amino-G Acid	44	34	165
2	KI0025F03:P7	23	Rhodamine WT	no bt	no bt	165
3	KI0025F03:P5	20	Uranine	31	-	164

R_i=recovery calculated by integration
R_w=recovery calculated by weighing
no bt= no breakthrough

Numerical modelling and analytical interpretation

The breakthrough curves from A-4 were evaluated using the one-dimensional advection-dispersion model described in Section 2.4.3.

The transport parameters derived from the numerical modelling and the analytical expressions described in Section 2.4.3 are presented in Table 3-12. A summary of hydraulic and transport parameters (from test A-4 and pre-test PT-4) for the flow paths tested using KI0023B:P6 as sink is presented in Table 3-13.

The best-fit runs for each tracer/flow path are presented in Figure 3-17. The modelling resulted in relatively good fits with quite low standard errors, 1-3 %.

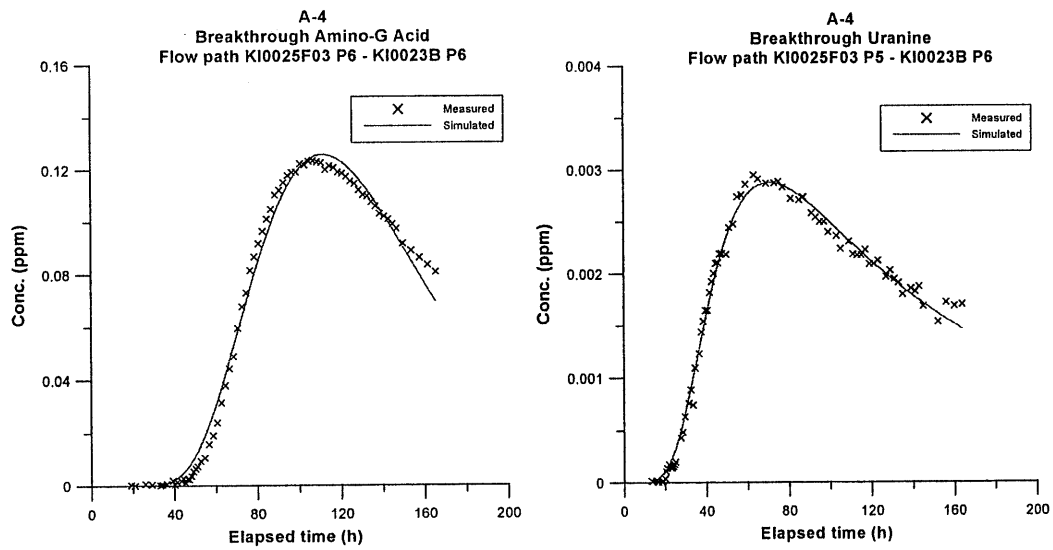

Figure 3-17. Comparison between measured and simulated tracer breakthrough in KI0023B:P6 during test A-4, cf. Table 3-12 for evaluated parameters. Note that the axis scales differ between the plots.

Table 3-12. Summary of hydraulic and transport parameters for the flow paths tested in A-4 using KI0023B:P6 as sink. Values within brackets are standard errors in percent.

Parameter	KI0025F03:P5 -KI0023B:P6 Value	KI0025F03:P6 -KI0023B:P6 Value	Source
Distance along fractures (m)	16	73	Geometry
Euclidean distance, L (m)	14	15	Geometry
Mean head difference, Δh (m)	177.4	193.7	HMS
Inj. flow rate (ml/h)	31	341	Injection curve
Mean velocity, v (m/s)	$5.01 \cdot 10^{-5}$ (1)	$3.83 \cdot 10^{-5}$ (1)	PAREST
Mean travel time, t_m (h)	77.7 (1)	108.8 (1)	PAREST
First arrival, t_a (h)	20	48	Breakthrough curve
Dispersivity, D/v (m)	3.1 (2)	1.2 (3)	PAREST
Peclet number, Pe	4.5	12.6	PAREST
Fracture conductivity, K_{fr} (m/s)	$1.2 \cdot 10^{-5}$	$8.9 \cdot 10^{-6}$	Eq. 2-7
Equivalent fracture aperture, b (m)	$1.7 \cdot 10^{-2}$	$2.1 \cdot 10^{-2}$	Eq. 2-8
Flow porosity (1 m thickness)	$9.4 \cdot 10^{-3}$	$12 \cdot 10^{-3}$	Eq. 2-9
Mass recovery, R (%)	>31	>44 >34*	Breakthrough curve

*=recovery calculated by weighing

Table 3-13. Summary of hydraulic and transport parameters for the flow paths tested using KI0023B:P6 as sink.

Parameter	KI0025F03: P5 - KI0023B:P6 Value	KI0025F03: P6 - KI0023B:P6 Value	KA2563A:S4 - KI0023B:P6 Value	KI0025F02: P6 - KI0023B:P6 Value	KI0025F02: P3 - KI0023B:P6 Value
Distance along fractures (m)	16	73	16	65	33
Euclidean distance, L (m)	14	15	16	18	36
Mean head difference, Δh (m)	177	194	190	204	215
Inj. flow rate (ml/h)	31	341	680	350	113
Mean travel time, t_m (h)	78	109	11.5	98	140
First arrival, t_a (h)	20	48	4	19	85
Dispersivity, D/v (m)	3.1	1.2	5.3	5.0	2.9
Equivalent fracture aperture, b (m)	$1.7 \cdot 10^{-2}$	$2.1 \cdot 10^{-2}$	$0.2 \cdot 10^{-2}$	$1.4 \cdot 10^{-2}$	$0.5 \cdot 10^{-2}$
Flow porosity (1 m thickness)	$9.4 \cdot 10^{-3}$	$12 \cdot 10^{-3}$	$1.1 \cdot 10^{-3}$	$8.0 \cdot 10^{-3}$	$2.7 \cdot 10^{-3}$
Mass recovery, R (%)	>31	>44 >34*	51	>80	>75

*=recovery calculated by weighing

3.7 Test A-5

The fifth test, A-5, was focused on tracer transport. Based on the many good flow responses observed during test A-1 (Table 3-2) the same set-up was decided for use in A-5. Pumping was done in KI0025F03:P5 (structure #20) using maximum possible flow, 2.6 l/min, and five injection sections were chosen (Table 3-14).

3.7.1 Tracer injections

The injections were performed as decaying pulses. The injection concentrations and injection rates given in Table 3-14 are the actually measured ones.

Table 3-14. Tracer injection data for test A-5 (measured values).

Inj #	Section	Structure #	Tracer	Max inj. conc (mg/l)	Inj rate (ml/h)*	Inj mass (mg)	Section Volume (ml)
1	KI0025F02:P3	13, 21	Uranine	460	120	3535[1] 4246[2]	8424
2	KI0025F02:P5	20	Naphtionate	650	536	4609[1] 5930[2]	6110
3	KI0025F02:P6	22	Rhodamine WT	120	1090	1312[1] 1961[2]	9916
4	KI0025F03:P6	22	Amino-G Acid	635	328	3525[1] 5146[2]	5687
5	KA2563A:S4	20	Rhodamine WT	260	570	1987[1] 2700[2]	6883

*Calculated from the tracer dilution during injection
[1]=calculated by integration
[2]=calculated by weighing

The injection functions presented as the logarithm of concentration (Ln C) versus time are shown in Figure 3-18.

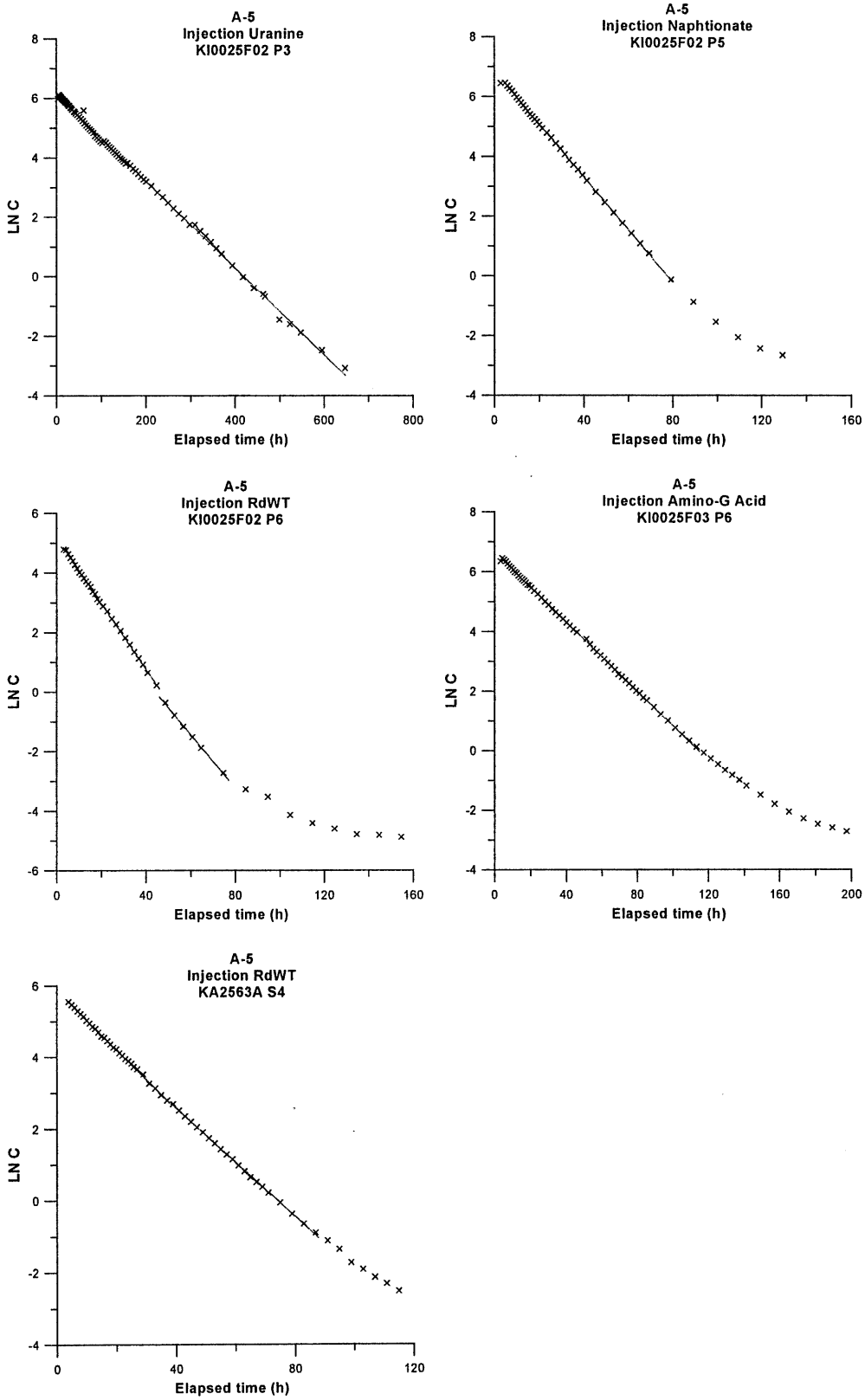

Figure 3-18. Tracer injection functions (Ln C versus time) including straight-line fits for the five injections during test A-5. Note that the axis scales differ.

3.7.2 Tracer breakthrough

The breakthrough of tracer was monitored both in the sink section KI0025F03:P5 and in borehole section KI0023B:P7 where the short-circuit between structure #6 and #20 occurs. Tracer breakthrough in section KI0025F03:P5 was detected from four of the five injections performed and the resulting breakthrough curves are presented in Figure 3-19. The breakthrough and injection curves are also plotted together (as mass flux versus time, log-log) in the same plot in Appendix 1. There was no breakthrough detected from the tracer Uranine injected in section KI0025F02:P3. No tracer breakthrough was found in KI0023B:P7 during the pumping period.

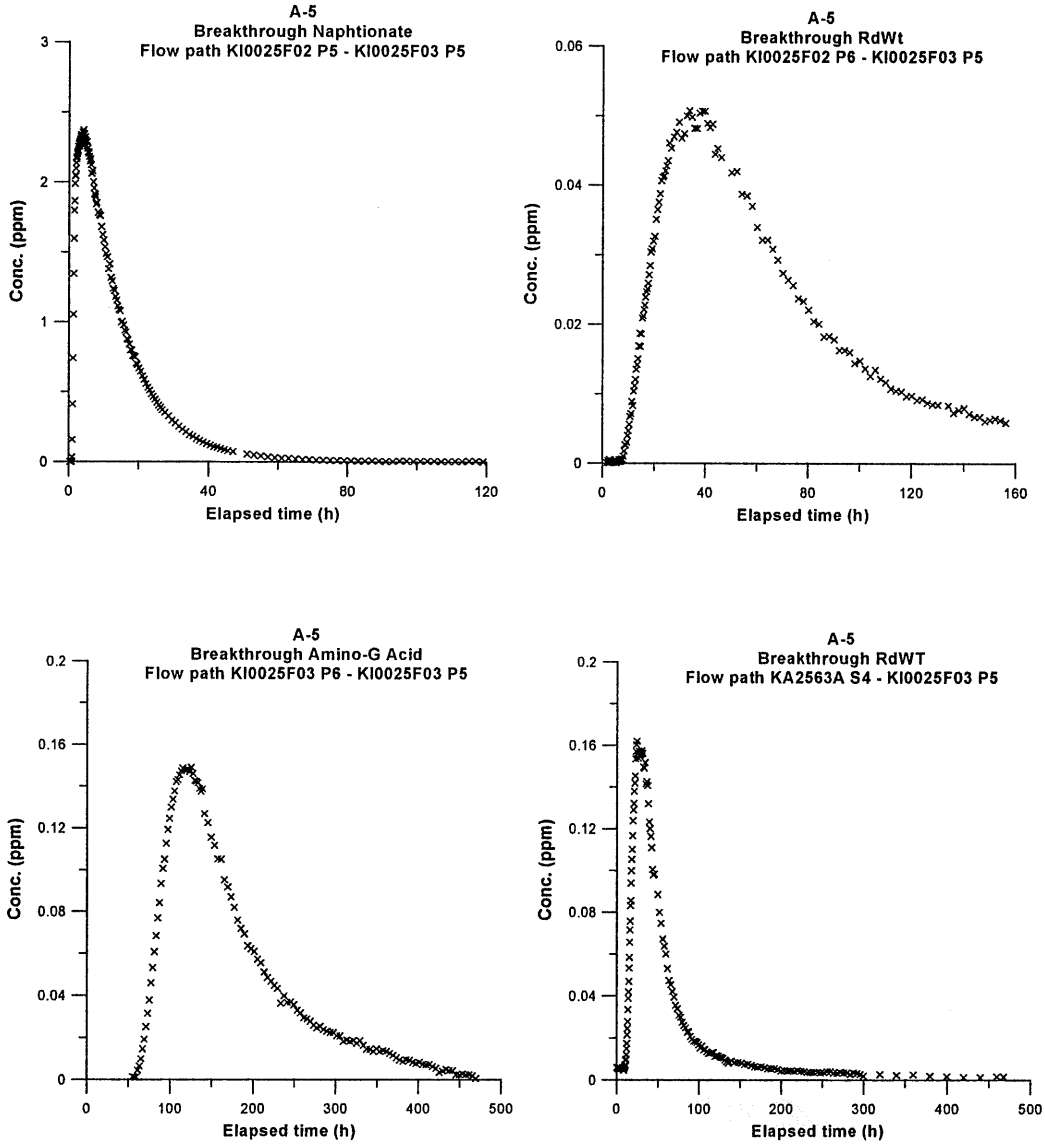

Figure 3-19. Tracer breakthrough in KI0025F03:P5 during test A-5. Note that the axis scales differ between the plots.

The pumping was stopped on January 14th, 2000 after a pumping period of 38 days. The equipment was removed to Uppsala for cleaning and maintenance. No major equipment failure occurred during the test period.

Tracer mass recovery was calculated in two different ways. Common for both methods was that the tracer mass recovered in the pumping borehole was determined by integration of the breakthrough curves for mass flux (mg/h) versus time (h). The injected mass was determined in the same way but also by weighing the tracer solution vessel during the injection procedure. The calculated injected masses, both integrated and weighed, are shown in Table 3-14.

The mass recoveries calculated from integration were constantly higher than the ones calculated by weighing (Table 3-15). In one case, Naphtionate injected in KI0025F02:P5, the recovery calculated from integration was >100 % which is unrealistic. One explanation for this may be that a larger volume is injected in the section (5-10 ml/min) than it is possible to withdraw with the sampling equipment (1.67 ml/min). This creates an overpressure and tracer solution is pushed into the fracture and is never counted for in the samples and concentration measurements. The injected mass determined by integration is then underestimated resulting in too high figures of the mass recoveries.

Calculations of the tracer mass recovery (Table 3-15) show high mass recovery for Naphtionate injected in KI0025F02:P5. The tracer mass recovery for Amino-G Acid (KI0025F03:P6) was, when calculated by integration, quite high, but was much lower when calculated by weighing. The mass recovery of Rhodamine WT from KI0025F02:P6 only reaches about 30-40 % . A portion of the tail of the breakthrough then still remains to be recovered though it is not likely the tracer mass recovery would have raised up to 100 %. The mass recovery of Rhodamine WT from KA2563A:S4 only reaches about 50-60 % which is in the same order as in PT-4, 50 %, (Andersson et al., 1999) and as in the combined interference and tracer tests, 44 %, (Andersson et al., 1998) but then another sink was used (KI0023B:P6). The pumping flow was during PT-4 2.5 l/min compared to 2.3 l/min in A-5. Finally, no breakthrough of Uranine from KI0025F02:P3 was detected when sampling stopped after 640 hours.

Table 3-15. Tracer mass recoveries from pumping section KI0025F03:P5 during test A-5.

Inj #	Section	Structure #	Tracer	R_i (%)	R_w (%)	Sampling time (h)
1	KI0025F02:P3	13, 21	Uranine	no bt	no bt	639
2	KI0025F02:P5	20	Naphtionate	125	97	157
3	KI0025F02:P6	22	Rhodamine WT	40	27	156
4	KI0025F03:P6	22	Amino-G Acid	84	57	470
5	KA2563A:S4	20	Rhodamine WT	64	47	468

R_i=recovery calculated by integration
R_w=recovery calculated by weighing
no bt= no breakthrough

3.7.3 Numerical modelling and analytical interpretation

The breakthrough curves from A-5 were evaluated using the one-dimensional advection-dispersion model described in Section 2.4.3.

The transport parameters derived from the numerical modelling and the analytical expressions described in Section 2.4.3 are presented in Table 3-16.

The best-fit runs for each tracer/flow path are presented in Figure 3-20. The modelling resulted in relatively good fits with quite low standard errors, 1-4 %, except for the dispersivity for flow path KI0025F02:P5 - KI0025F03:P5 with an error of 11 %. In general the peak of the breakthrough curves is quite well fitted while the tail part is worse.

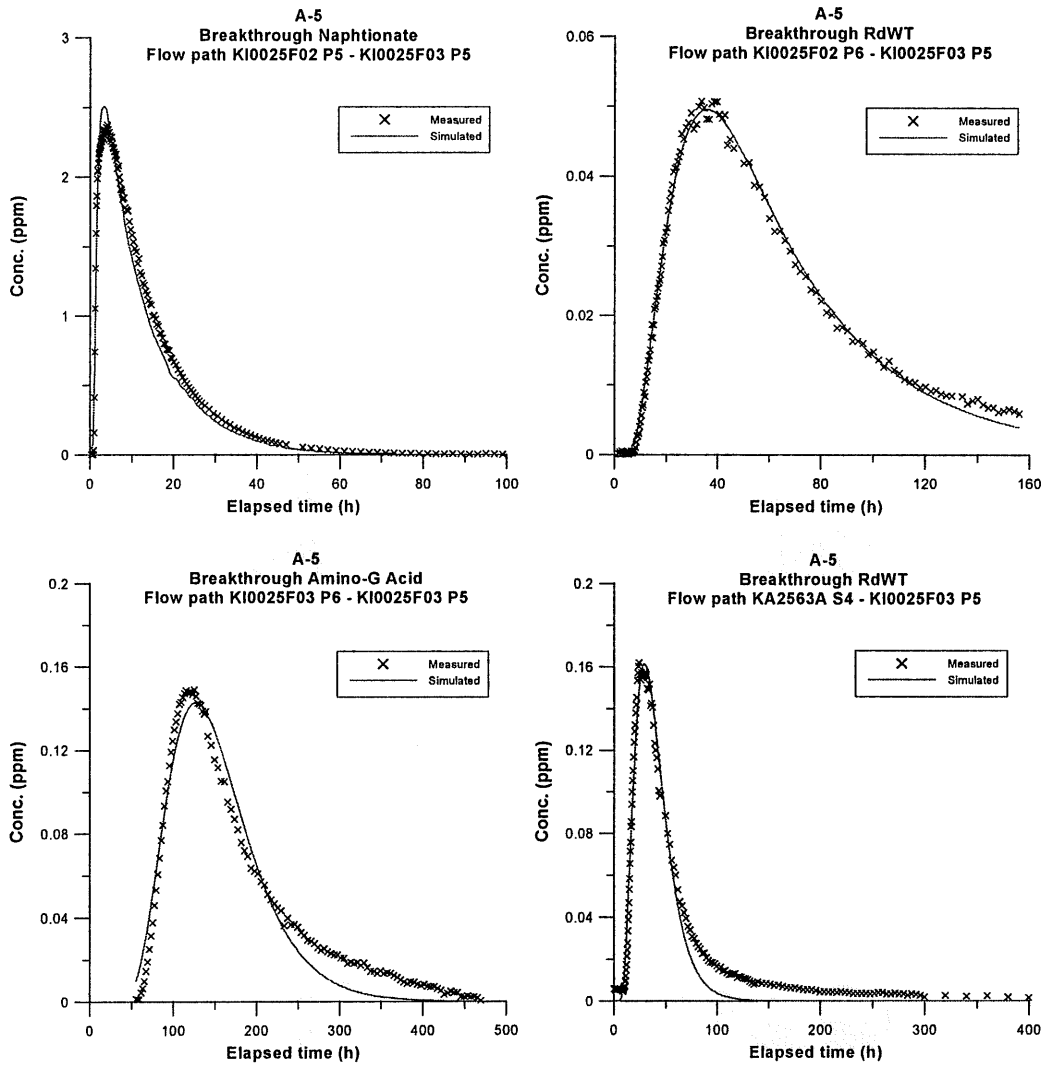

Figure 3-20. Comparison between measured and simulated tracer breakthrough in KI0025F03:P5 during test A-5, cf. Table 3-16 for evaluated parameters. Note that the axis scales differ between the plots.

Table 3-16. Summary of hydraulic and transport parameters for the flow paths tested in A-5 using KI0025F03:P5 as sink. Values within brackets are standard errors in percent.

Parameter	25F02:P5 -25F03:P5 Value	25F02:P6 -25F03:P5 Value	25F03:P6 -25F03:P5 Value	2563A:S4 -25F03:P5 Value	Source
Distance along fractures (m)	9	57	65	27	Geometry
Euclidean distance, L (m)	11	12	12	29	Geometry
Mean head difference, Δh (m)	214.4	227.9	236.8	217.5	HMS
Inj. flow rate (ml/h)	536	1090	327	570	Injection curve
Mean velocity, v (m/s)	$2.13 \cdot 10^{-3}$ (1)	$7.91 \cdot 10^{-5}$ (1)	$2.64 \cdot 10^{-5}$ (1)	$3.32 \cdot 10^{-4}$ (1)	PAREST
Mean travel time, t_m (h)	1.4 (1)	42.2 (1)	126.4 (1)	24.2 (1)	PAREST
First arrival, t_a (h)	1	8	60	10	Breakthrough curve
Dispersivity, D/v (m)	0.63 (11)	4.4 (1)	0.95 (4)	3.7 (4)	PAREST
Peclet number, Pe	17.5	2.7	12.7	7.8	PAREST
Fracture conductivity, K_{fr} (m/s)	$3.1 \cdot 10^{-4}$	$1.2 \cdot 10^{-5}$	$3.8 \cdot 10^{-6}$	$1.5 \cdot 10^{-4}$	Eq. 2-7
Equivalent fracture aperture, b (m)	$5.9 \cdot 10^{-4}$	$1.5 \cdot 10^{-2}$	$4.4 \cdot 10^{-2}$	$1.4 \cdot 10^{-3}$	Eq. 2-8
Flow porosity (7.5 m thickness)	$6.9 \cdot 10^{-5}$	$1.8 \cdot 10^{-3}$	$5.5 \cdot 10^{-3}$	$1.5 \cdot 10^{-4}$	Eq. 2-9
Mass recovery, R (%)	125 97*	>40 >27*	84 57*	64 47*	Breakthrough curve

*=recovery calculated by weighing

3.8 Short-term interference tests

Prior to tracer test A-5 a number of short-term interference tests were performed by subsequent opening of 5 selected borehole sections in KI0025F03. The test were made as a complement to the earlier performed short-term interference tests in the same borehole (Gentzschein & Ludvigson, 1999), which were made in twelve selected 2-m intervals. The new tests were performed by opening the flow lines connected to each monitoring section (with lengths between 3.5-7.5 m) completely (constant head), for a period of about 30 minutes. The flow from the section and the electrical conductivity were monitored after 1, 5, 10, 20 and 30 minutes of pumping. After shut-in, the pressure build-up was monitored for period of at least 60 minutes. A summary of the short-term interference tests is shown in Table 3-17.

Table 3-17. Summary of the short-term interference tests performed during TRUE Block Scale Tracer Test Stage.

Test #	Source section	Q_p* (l/min)	s_p ** (m)	Q_p/s_p (m^2/s)	Flow period (min)	Structure
25F3P3	KI0025F03:P3	0.43	406.5	$1.8 \cdot 10^{-8}$	32	#13
25F3P4	KI0025F03:P4	1.30	373.8	$5.8 \cdot 10^{-8}$	32	#21
25F3P5	KI0025F03:P5	3.0	272.4	$1.8 \cdot 10^{-7}$	32	#20
25F3P6	KI0025F03:P6	0.79	40.3	$3.3 \cdot 10^{-7}$	32	#22
25F3P7	KI0025F03:P7	0.52	401.7	$2.2 \cdot 10^{-8}$	32	#23

* Flow rate at the end of flowing period
** Drawdown at the end of flowing period

Only a qualitative evaluation was made for the short-term interference tests. The response diagrams are shown in Appendix 2. The pressure response matrix for these tests is shown in Figure 3-21. The figure shows that the test responses generally are consistent with the structural model (March 1999). However, the test in KI0025F03:P3 (structure #13) gave no responses in sections KA2563A:S3 and KI0023B:P4 both also interpreted to contain structure #13. The pressure response matrix for sections KI0025F03:P5 (#20) and KI0025F03:P4 (#21) could also be compared to Figure 3-1 and the pressure responses in tests A-1 and A-2 that used the same sinks.

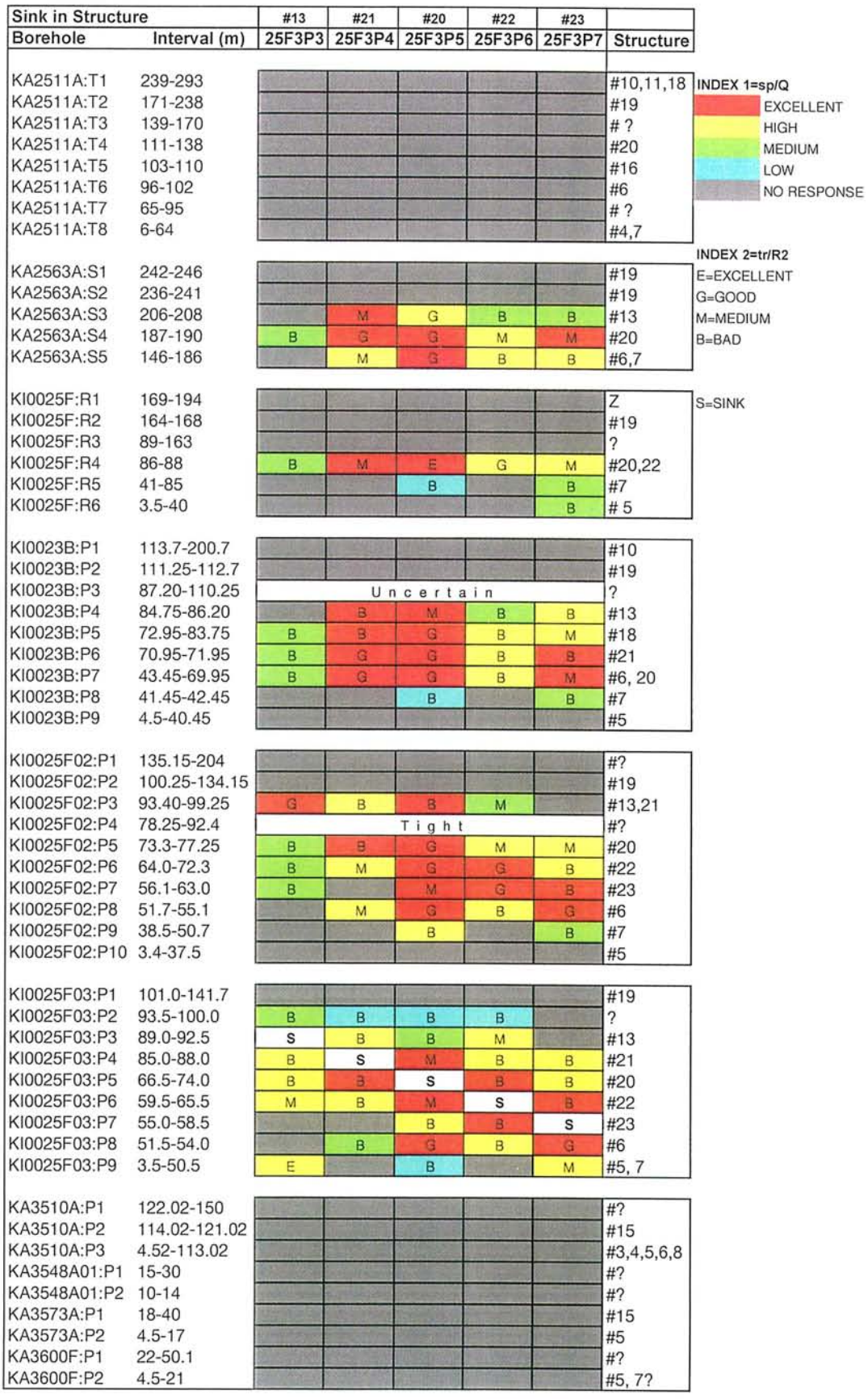

Figure 3-21. Pressure response matrix for the short-term interference tests.

4 Conclusions

4.1 Connectivity and structural model

The performed tests generally confirm the reconciled March'99 structural model and the conclusions from the short-term interference tests in KI0025F03 (Gentzschein & Ludvigson, 2000).

Test A-1, using section KI0025F03:P5 as sink, shows very good connectivity with the entire fracture system, in particular structures #20, 21, 22, 23 and 6, see Figure 2-2. The test confirms that the sink is located in structure #20. The groundwater flow measurements show significant responses in 11 out of 18 measured sections. The most significant flow responses are in general also found in sections with good pressure responses but there are two exceptions having low and slow pressure responses but high flow responses, KI0025F02:P3 and KI0025F03:P6. The former section, interpreted to be intersected by both structures #13 and 21, has been discussed by Doe (1999) who interpreted the low pressure response as a boundary effect caused by the closeness to a permeable boundary. The same explanation could also apply for KI0025F03:P6, which is close to the permeable structure #20.

Test A-2, performed by flowing section KI0025F03:P4 shows good pressure responses in structures #20, 21 and 6. Large drawdown but delayed responses are also found in sections including structures #13, 22 and 23. The radius of influence (corresponding to a drawdown >1 kPa) is smaller for test A-2 than for A-1, possibly indicating less good hydraulic connection within the structure(s) tested. The test confirms that the sink section is located in structure #21. The groundwater flow measurements generally show better responses in structures #21, 19 and 13 than in test A-1 (and A-3) but lower responses in structures #6, 20, 22 and 23 which is in agreement with the structural model. Section KI0023B:P5 also responds very good to test A-2 indicating that this section is well connected to structure #13 and/or #21 which is consistent with previous tests and conclusions by Doe (1999).

Test A-3, using section KI0025F02:P5 as sink, is almost a mirror image of test A-1 both in terms of pressure responses and in flow responses and the same conclusions as in test A-1 are valid also for A-3.

Test A-4, using section KI0023B:P6 as sink, also shows a response pattern similar to test A-1 and A-3. This test has been performed and evaluated during the Pre-Tests (Andersson et al., 1999) but test A-4 included additional groundwater flow measurements in five sections of KI0025F03. The flow responses were found to be almost identical to the ones in test A-1 and A-3.

The short-term tests performed in KI0025F03 shows that the test responses generally are consistent with the structural model (March 1999). The only inconsistency is that

the test in KI0025F03:P3 (structure #13) gave no responses in sections KA2563A:S3 and KI0023B:P4 both also interpreted to contain structure #13.

Based on the results from test A-1 to A-3, the best sink to use as an alternative to KI0023B:P6 was selected for test A-5. As test A-2 showed somewhat less good connectivity the final choice was between the A-1 and A-3 sinks, KI0025F03:P5 and KI0025F02:P5, both located within structure #20. Both these sinks have a very similar response pattern, both in terms of flow and pressure, which made it difficult to choose. The final choice fell on the A-1 sink, KI0025F03:P5 based on i) the possibility to address the effects of fracture intersections , ii) that some of the sections with very good flow responses are located in KI0025F02 and therefore would be easier to use as potential injection points (better defined flow path).

4.2 Hydraulic parameters

The quantitative analysis of the most prominent pressure responses in all tests generally shows a short period o (pseudo)-radial flow transiting to leaky (pseudo-spherical) flow. Towards the end of the flow period, a virtually steady-state flow occurred in all sections analysed (4-7 sections during each test). The parameter values determined for transmissivity, T, storativity, S, hydraulic diffusivity, T/S, and leakage coefficient, K′/b′, were generally within a relatively narrow range, see Table 4-1. The only notable differences are that the transmissivity for structure #13 are somewhat lower than for structures #20, 21 and 6 and that the leakage coefficient is higher for structure #6.

Table 4-1. Summary of results of selective time-drawdown analysis for test A-1 to A-4 (sinks not included)

.Structure #	# of tests evaluated	T (m^2/s)	S	T/S (m^2/s)	K′/b′ (s^{-1})
20	9	$5.2\text{-}7.9\cdot10^{-7}$	$0.7\text{-}8.6\cdot10^{-7}$	0.6-11	$0.7\text{-}5.2\cdot10^{-11}$
21	4	$7.3\text{-}7.6\cdot10^{-7}$	$2.4\text{-}11\cdot10^{-7}$	0.7-3.0	$1.3\text{-}5.2\cdot10^{-11}$
13	2	$2.0\text{-}2.1\cdot10^{-7}$	$4.1\text{-}8.2\cdot10^{-7}$	0.2-0.5	$2.6\text{-}3.9\cdot10^{-11}$
6	1	$1.5\cdot10^{-6}$	$8.4\cdot10^{-7}$	1.8	$5.7\cdot10^{-10}$
18*	1	$6.8\cdot10^{-7}$	$8.2\cdot10^{-7}$	0.8	$6.9\cdot10^{-11}$

* structure in section KI0023B:P5

4.3 Transport parameters

The tracer dilution tests in 53 different sections showed that the "natural" flow varies quite a lot within the Block Scale rock volume. An extremely high flow rate (11 l/h) was measured in KI0023B:P7 where a short-circuit between structures #6 and #20 exists as previously discussed in Andersson et al. (1999). The flow rates in the other

measured sections typically were in the range 0-300 ml/h. There are also variations in the "natural" flow between the different tests for some sections.

Based on the measured flow rates, the Darcy velocity was estimated as described in Chapter 2.4.2. The Darcy velocities determined together with estimates of the hydraulic conductivity, presented in Table 4-1, where used to calculate the hydraulic gradient, *I*. The estimated gradients are typically in the order of 0.3-3 m/m. The exceptions are some sections connected to structures #13, #20 and #21 having a lower gradient, a somewhat higher gradient in sections KI0025F02:P6 (#22) and KI0025F02:P7 (#23) and an extremely high gradient in the short-circuit section KI0023B:P7 (#6, 20).

The tracer test in A-4 performed by pumping in structure #21 (KI0023B:P6) resulted in tracer breakthrough from two of three injection points, KI0025F03:P5 (structure #20) and KI0025F03:P6 (#22). No breakthrough was observed from injection in section KI0025F03:P7 (#23). The tests cover Euclidean distances ranging between 14 to 17 m which probably are longer in reality. The tracer mass recoveries are not very high (30-40 %) but a large portion of the tail of the breakthrough curves still remained to be recovered when sampling was finished, and therefore it is likely that the mass recoveries would have increased by another 20-30 %. The numerical modelling using a simple one-dimensional advection-dispersion model was able to fit the breakthrough curves quite well with low standard errors. The transport parameters calculated based on the mean travel times; fracture conductivity, equivalent fracture aperture and flow porosity, are in the same order of magnitude for both flow paths investigated.

The tracer test in A-5 performed by pumping in structure #20 (KI0025F03:P5) resulted in tracer breakthrough from four of five injection points, KI0025F02:P5 (structure #20), KI0025F02:P6 (#22), KI0025F03:P6 (#22) and KA2563A:S4 (#20). No breakthrough was observed from injection in section KI0025F02:P3 (#13, 21). The tests cover Euclidean distances ranging between 11 to 29 m which probably are longer in reality.

The tracer mass recoveries were calculated in two different ways, using injected mass estimated by integration or by weighing. The recoveries determined from integration were constantly higher than the ones calculated by weighing. The mass recovery in test A-5 from the injection in KI0025F02:P5 determined from integration was >100 %. Calculated by weighing it was still very high, 97 %. The injection in KI0025F03:P6 gave an "integrated" high recovery of 84 % while the "weighed" recovery was just 57 %. The mass recovery from injection in KI0025F02:P6 only reaches about 30-40 % with a portion of the tail of the breakthrough still left to be recovered. However, it is not likely the recovery would have raised up to 100 % even with a complete breakthrough curve. The long flow path from KA2563A:S4 only gave a recovery of about 50-60 % which is in the same order as in PT-4 (50 %) and as in the combined interference and tracer tests (44 %) even though another sink then was used (KI0023B:P6).

The numerical modelling using a simple one-dimensional advection-dispersion model resulted in relatively good fits with quite low standard errors, 1-4 %, except for the dispersivity for flow path KI0025F02:P5 - KI0025F03:P5 with an error of 11 %. In general the peak of the breakthrough curves is quite well fitted while the tail part is worse. This is not surprising as the model is extremely simple. The fits could easily have been improved just by adding one or two extra flow paths but this was outside the scope of this part of the project. The transport parameters calculated based on the mean

travel times; fracture conductivity, equivalent fracture aperture and flow porosity, show somewhat different values, where the flow path from KI0025F03:P6 shows a slow transport, indicating high flow porosity (and large equivalent aperture) whereas the very fast flow path from KI0025F02:P5 has about two orders of magnitude lower flow porosity (and equivalent aperture).

Table 4-1. Summary of calculated Darcy velocities and hydraulic gradients from tests A-1 to A-4.

Section	Structure #	Darcy velocity (m/s)	Hydraulic conductivity* (m/s)	Hydraulic gradient (m/m)
KI0025F02:P8	6	$3.3\text{-}4.0\cdot10^{-9}$	$3.2\cdot10^{-9}$	1.0-1.2
KA2563A:S3	13	$0.4\text{-}1.2\cdot10^{-8}$	$1.4\cdot10^{-8}$	0.3-0.9
KI0023B:P4	13	$2.8\text{-}6.7\cdot10^{-9}$	$1.9\cdot10^{-8}$	0.1-0.3
KI0025F03:P3	13	$0.0\text{-}8.9\cdot10^{-9}$	$3.9\cdot10^{-9}$	0-2.3
KI0023B:P5	18	$8.0\text{-}8.6\cdot10^{-10}$	$1.6\cdot10^{-9}$	0.5-0.6
KA2563A:S1	19	$1.3\text{-}4.5\cdot10^{-8}$	$2.4\cdot10^{-8}$	0.6-1.9
KI0023B:P2	19	$2.0\text{-}2.5\cdot10^{-8}$	$6.8\cdot10^{-8}$	0.3-0.4
KA2563A:S4	20	$1.7\cdot10^{-7}$	$6.3\cdot10^{-8}$	2.6
KI0025F02:P5	20	$0.5\text{-}1.0\cdot10^{-8}$	$3.0\cdot10^{-8}$	0.2-0.3
KI0025F03:P5	20	$0.0\text{-}1.1\cdot10^{-9}$	$2.2\cdot10^{-8}$	0-0.05
KI0023B:P6	21	$0.8\text{-}3.8\cdot10^{-8}$	$1.3\cdot10^{-7}$	0.06-0.3
KI0025F03:P4	21	$0.6\text{-}9.7\cdot10^{-9}$	$1.4\cdot10^{-8}$	0.04-0.7
KI0025F02:P6	22	$3.0\text{-}5.9\cdot10^{-8}$	$1.2\cdot10^{-8}$	2.5-4.9
KI0025F03:P6	22	$1.9\text{-}2.5\cdot10^{-8}$	$4.7\cdot10^{-8}$	0.4-0.5
KI0025F02:P7	23	$0.2\text{-}1.2\cdot10^{-8}$	$7.8\cdot10^{-10}$	3-15
KI0025F03:P7	23	$1.1\text{-}1.4\cdot10^{-8}$	$4.7\cdot10^{-9}$	2.3-3.0
KI0025F:R4	20, 22	$1.6\text{-}5.4\cdot10^{-9}$	$1.8\cdot10^{-8}$	0.1-0.3
KI0023B:P7	6, 20	$7.6\cdot10^{-7}$	$3.8\cdot10^{-9}$	202
KI0025F02:P3	13, 21	$0.8\text{-}1.4\cdot10^{-8}$	$5.4\cdot10^{-9}$	1.4-2.6

*=determined from detailed flow logging

4.4 Choice of sink for tracer tests during Phase B and C

Based on the results from the analysis of the tracer tests performed during tests A-4 and A-5 together with previous tracer tests performed (PT-4, Andersson et al., 1999) a final choice of sink for the planned tracer test during Phase B and C of the Tracer Test Stage was done. The planned tests include injections of radioactive sorbing tracers that require high mass recovery and good control of the experiments. Test A-5 only gives one or maybe two flow paths with high enough mass recovery whereas test A-4, using KI0023B:P6 as sink gave at least four possible injection points. Thus, the latter sink is suggested to use for the planned tracer tests in Phase B and C.

5 References

Andersson, P., 1996: TRUE 1st stage tracer test programme. Experimental data and preliminary evaluation of the TRUE-1 radially converging tracer test (RC-1). Äspö Hard Rock Laboratory Progress Report HRL-96-24.

Andersson, P., Ludvigson, J-E., Wass, E., 1998: TRUE Block Scale Project, Preliminary Characterisation Stage. Combined Interference Tests and Tracer Tests. Appendix volume. Evaluation plots and data sheets for interference test interpretation. Äspö Hard Rock Laboratory Technical Note TN-98-28b.

Andersson, P., Ludvigson, J-E., Wass, E., Holmqvist, M., 1999: TRUE Block Scale Project, Detailed Characterisation Stage. Interference tests and tracer tests, PT-1 - PT-4. Äspö Hard Rock Laboratory International Technical Document ITD-99-19.

Andersson, P., Ludvigson, J-E., 2000: TRUE Block Scale Project: Tracer dilution tests during pumping in borehole KI0023B and short term interference tests in KI0025F02 and KA3510A. Äspö Hard Rock Laboratory International Technical Document, ITD-00-02.

Cooper, H.H. Jr., Jacob, C.E., 1946: A Generalized Graphical Method for Evaluating Formation Constants and Summarizing Well-Field History. Am. Geophys. Union Trans., Vol. 27, No. 4, pp. 526-534.

Doe, T., 1999: TRUE Block Scale Project. Reconciliation of the March'99 structural model and hydraulic data. Äspö HRL International Technical Document ITD-99-20.

Gentzschein, B., Ludvigson, J-E., 2000: Single-hole hydraulic tests and short-term interference tests in KI0025F03. Äspö Hard Rock Laboratory International Technical Document, ITD-00-05.

Gustafsson, E., Klockars, C-E., 1981: Studies of groundwater transport in fractured crystalline rock under controlled conditions using non-radioactive tracers. Swedish Nuclear Fuel and Waste Management Company. SKBF/KBS Technical Report TR 81-07.

Hantush, M.S., Jacob, C.E., 1955: Non-steady radial flow in an infinite leaky aquifer. Am. Geophys. Union Trans., Vol. 36, pp. 95-100.

Hermanson, J., in prep.: TRUE Block Scale Project. Structural model March 1999; based on borehole data from KI0025F02, KA3600F and KA3573A. Äspö Hard Rock Laboratory International Technical Document, in prep.

Moye, D.G., 1967: Diamond drilling for foundation exploration. Civil Eng. Trans., Inst. Eng. Australia (Apr. 1967), 95-100.

Nordqvist, R., 1994: Documentation of some analytical flow and transport models implemented for use with PAREST - Users manual. GEOSIGMA GRAP 94 006, Uppsala.

Ogata, A., Banks, R., 1961: A solution to the differential equation of longitudinal dispersion in porous media. U.S. Geol. Surv. Prof. Paper 411-A, Washington.

Rhén, I., Forsmark, T., Gustafson, G., 1991: Transformation of dilution rates in borehole sections to groundwater flow in the bedrock. Technical Note 30. In: Liedholm, M. (ed), 1991: SKB-Äspö Hard Rock Laboratory, Conceptual Modeling of Äspö, Technical Notes 18-32. General Geological, Hydrogeological and Hydrochemical information. Swedish Nuclear Fuel and Waste Management Company. Äspö Hard Rock Laboratory Progress Report PR 25-90-16 b.

Theis, C.V., 1935: The Relationship Between the Lowering of the Piezometric Surface and the Rate and Duration of Discharge Using Groundwater Storage. Trans. Am. Geophys. Union, Vol. 16, pp. 519-524.

Van Genuchten, M.Th., 1982: One-dimensional analytical transport modeling, in Proceedings: Symposium on unsaturated flow and transport modeling. Rep. PNL-SA-10325, Pacific Northwest Lab., Richland, Washington

Van Genuchten M.Th., and Alves, W.J., 1982: Analytical solutions of the one-dimensional convective-dispersive solute transport equation. U.S. Dep. Agric. Tech. Bull. 1661.

Waterloo Hydrogeologic Inc. Aquifer Test version 2.0.

Winberg A. (ed), 1996: First TRUE Stage - Tracer Retention Understanding Experiments. Descriptive structural-hydraulic models on block and detailed scales of the TRUE-1 site. Swedish Nuclear Fuel and Waste Management Company. Äspö Hard Rock Laboratory International Cooperation Report ICR 96-04.

Winberg, A., 1997: Test plan for the TRUE Block Scale Experiment. Äspö Hard Rock Laboratory. Äspö HRL International Cooperation Report ICR 97-02.

Winberg, A. (ed) 2000 : TRUE Block Scale Project. Tracer Test Stage. Compilation of premises and outline of programme for tracer tests in the Block Scale. Äspö Hard Rock Laboratory. Äspö HRL International Cooperation Report ICR-00-02.

Zuber, A., 1974: Theoretical possibilities of the two-well pulse method. Isotope Techniques in Groundwater Hydrology 1974, Proc. Symp., Vienna 1974, IAEA, Vienna

APPENDIX 1: Breakthrough and injection curves as mass flux versus time for A-4 and A-5

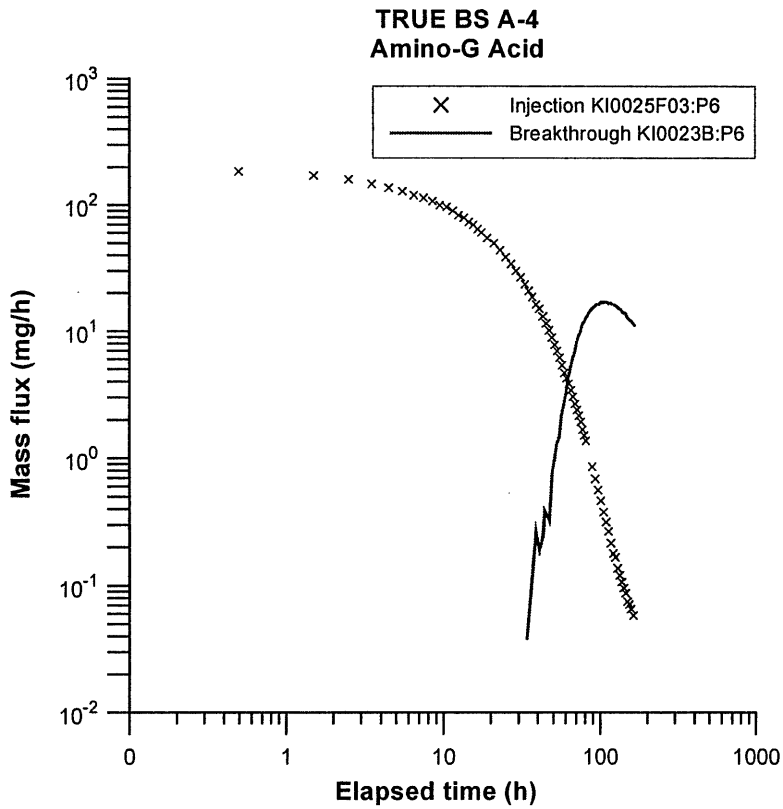
TRUE BS A-4
Amino-G Acid
Injection KI0025F03:P6
Breakthrough KI0023B:P6
Mass flux (mg/h)
Elapsed time (h)
10^3
10^2
10^1
10^0
10^-1
10^-2
0
1
10
100
1000

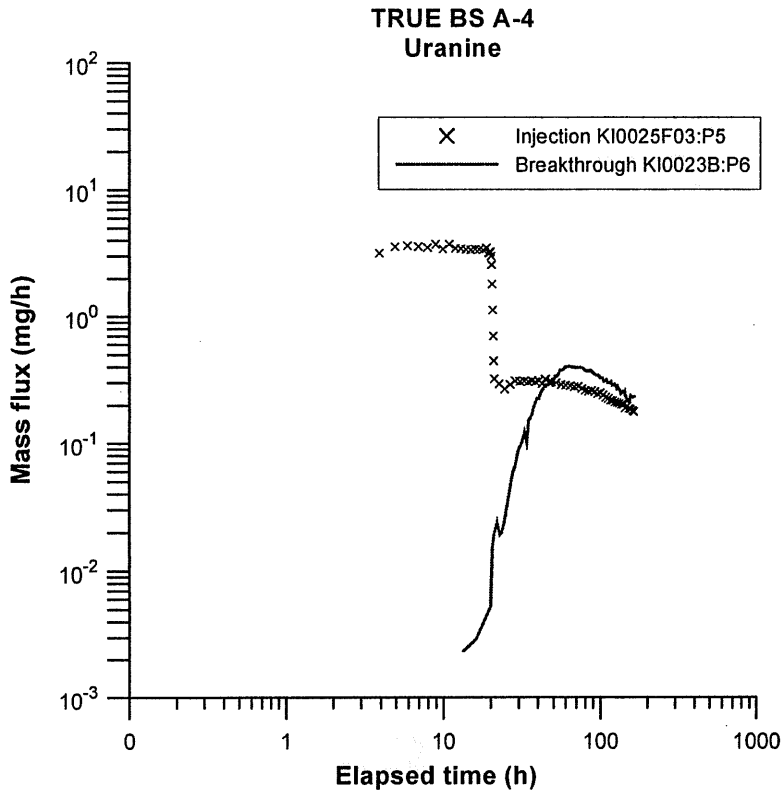
TRUE BS A-4
Uranine
Injection KI0025F03:P5
Breakthrough KI0023B:P6
Mass flux (mg/h)
Elapsed time (h)
10^2
10^1
10^0
10^-1
10^-2
10^-3
0
1
10
100
1000

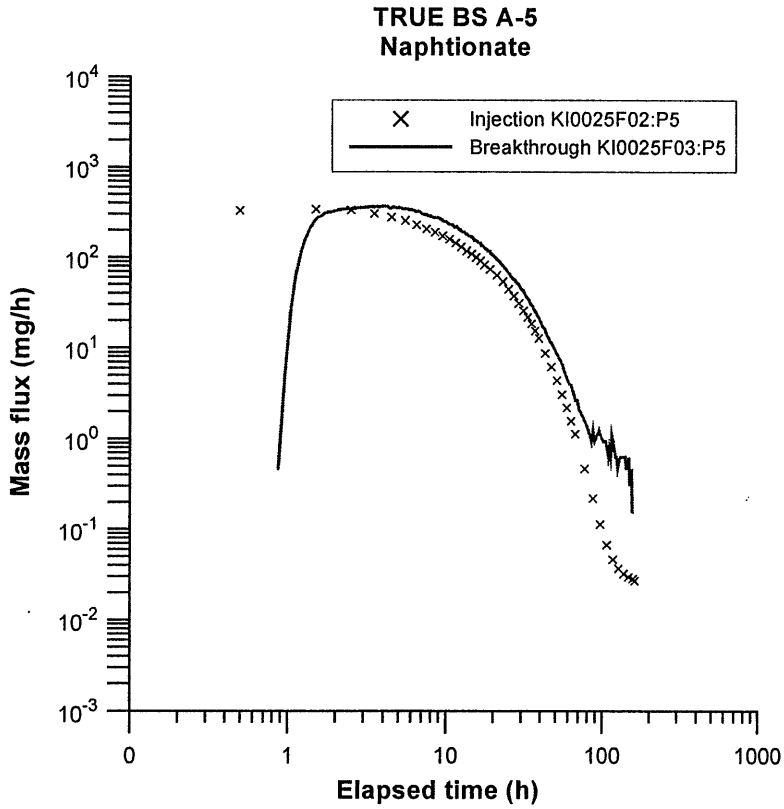
TRUE BS A-5
Naphtionate
Injection KI0025F02:P5
Breakthrough KI0025F03:P5
Mass flux (mg/h)
Elapsed time (h)

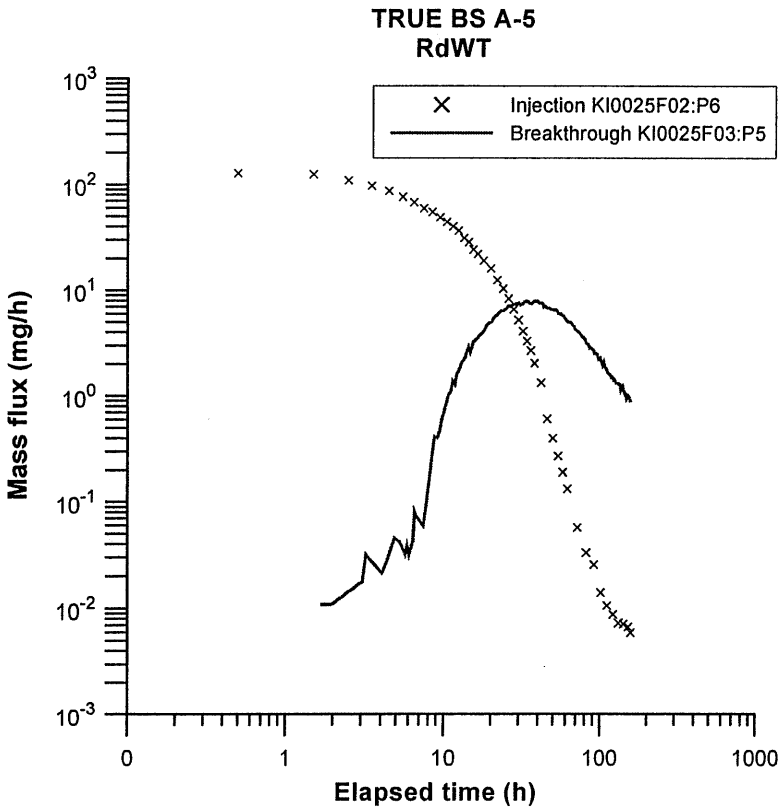
TRUE BS A-5
RdWT
Injection KI0025F02:P6
Breakthrough KI0025F03:P5
Mass flux (mg/h)
Elapsed time (h)

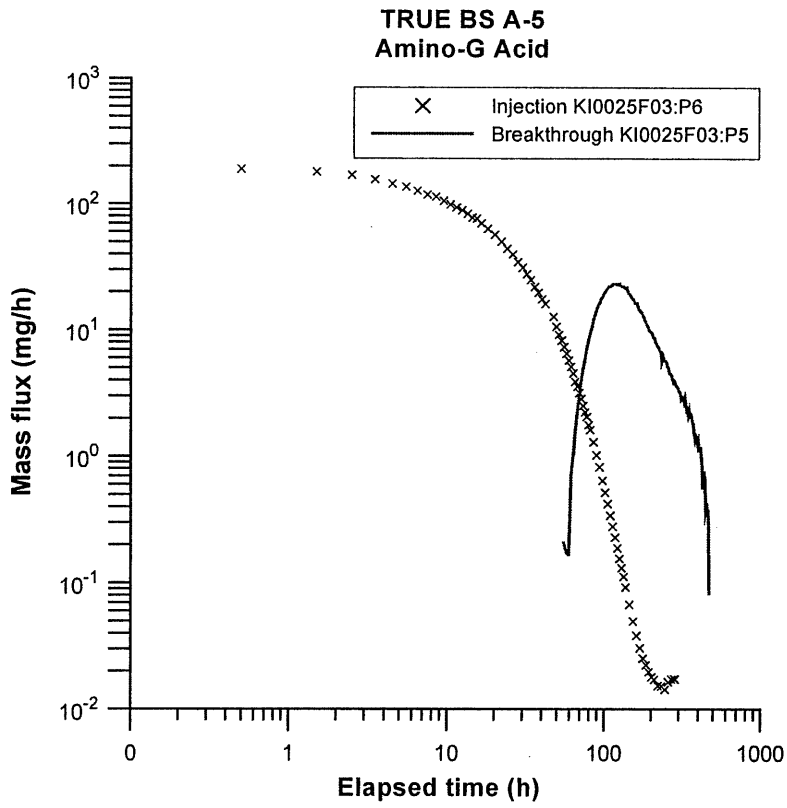
TRUE BS A-5
Amino-G Acid
Injection KI0025F03:P6
Breakthrough KI0025F03:P5
Mass flux (mg/h)
Elapsed time (h)
10^3
10^2
10^1
10^0
10^-1
10^-2
0
1
10
100
1000

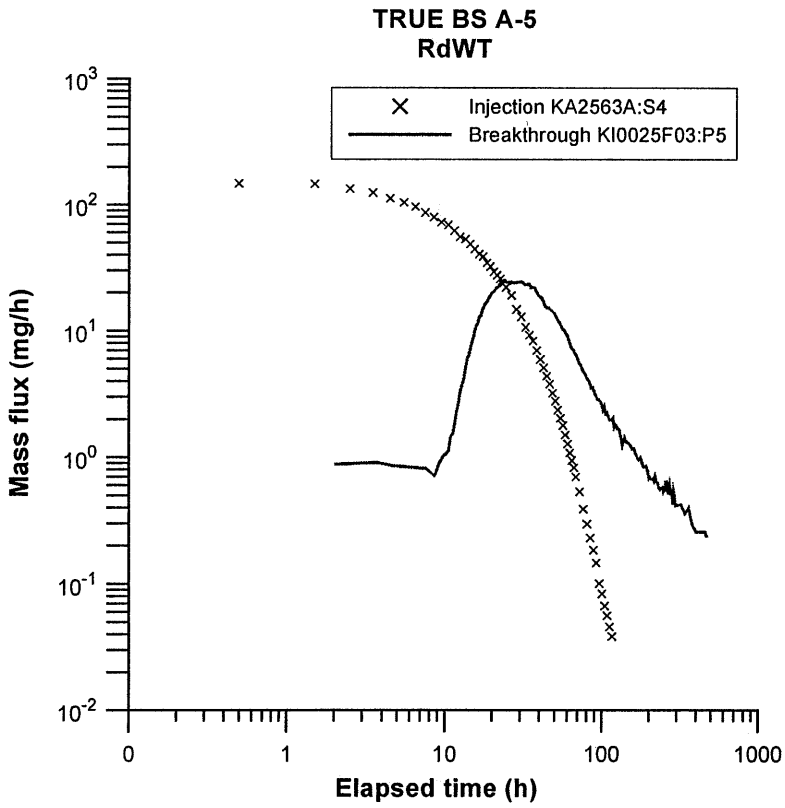
TRUE BS A-5
RdWT
Injection KA2563A:S4
Breakthrough KI0025F03:P5
Mass flux (mg/h)
Elapsed time (h)
10^3
10^2
10^1
10^0
10^-1
10^-2
0
1
10
100
1000

APPENDIX 2: Pressure response diagrams for the short-term interference tests in KI0025F03

TRUE Block Scale. Short Term Interference Test - Sink: KI0025F03:P3 (89.0-92.5 m). Structure #13
Most significant responses (>1 kPa)

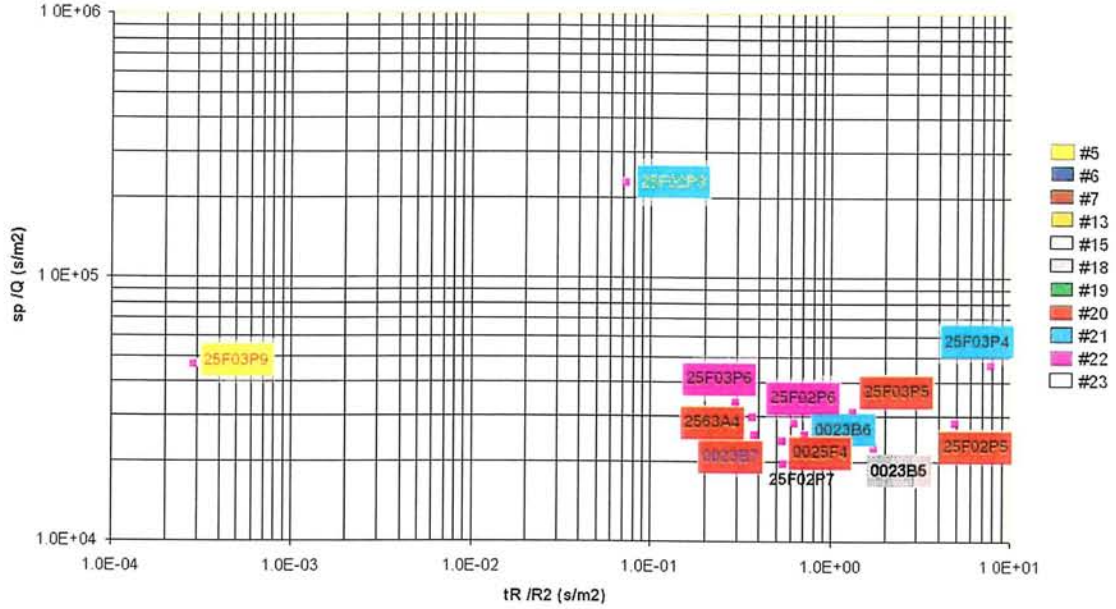

TRUE Block Scale. Short Term Interference Test - Sink: KI0025F03:P4 (85.0-88.0 m). Structure #21
Most significant responses (>1 kPa)

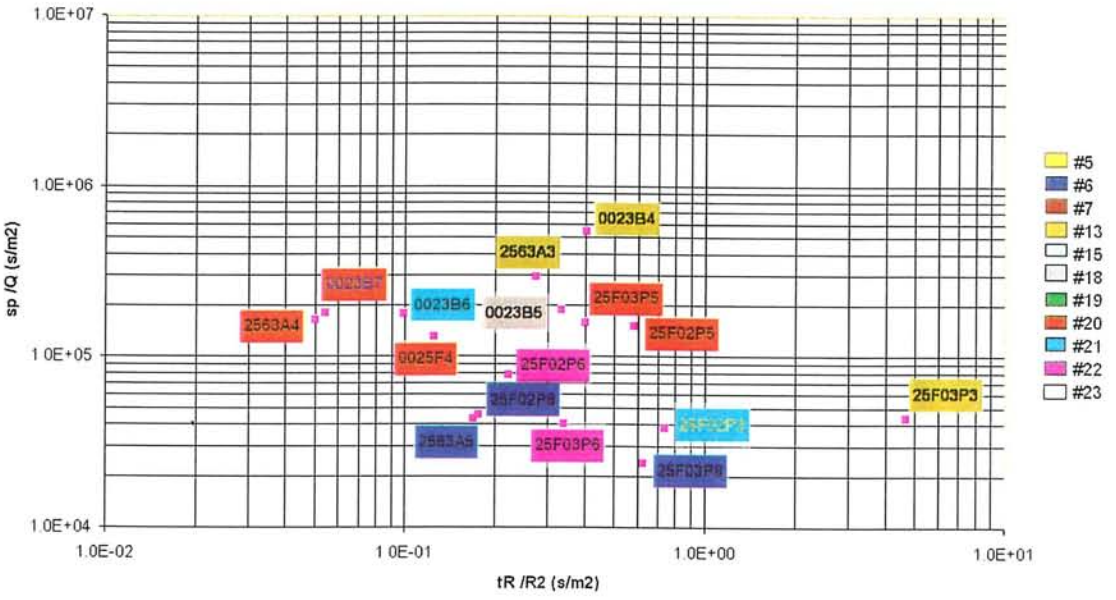

TRUE Block Scale. Short Term Interference Test - Sink: KI0025F03:P5 (66.5-74.0 m). Structure #20
Most significant responses (>1 kPa)

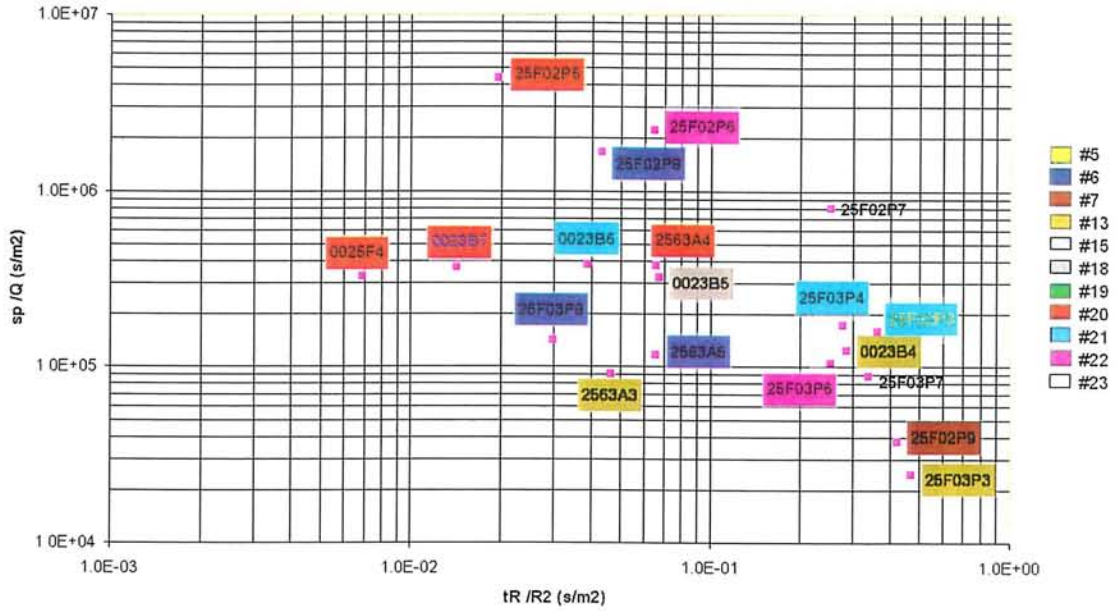

TRUE Block Scale. Short Term Interference Test - Sink: KI0025F03:P6 (59.5-65.5 m). Structure #22
Most significant responses (>1 kPa)

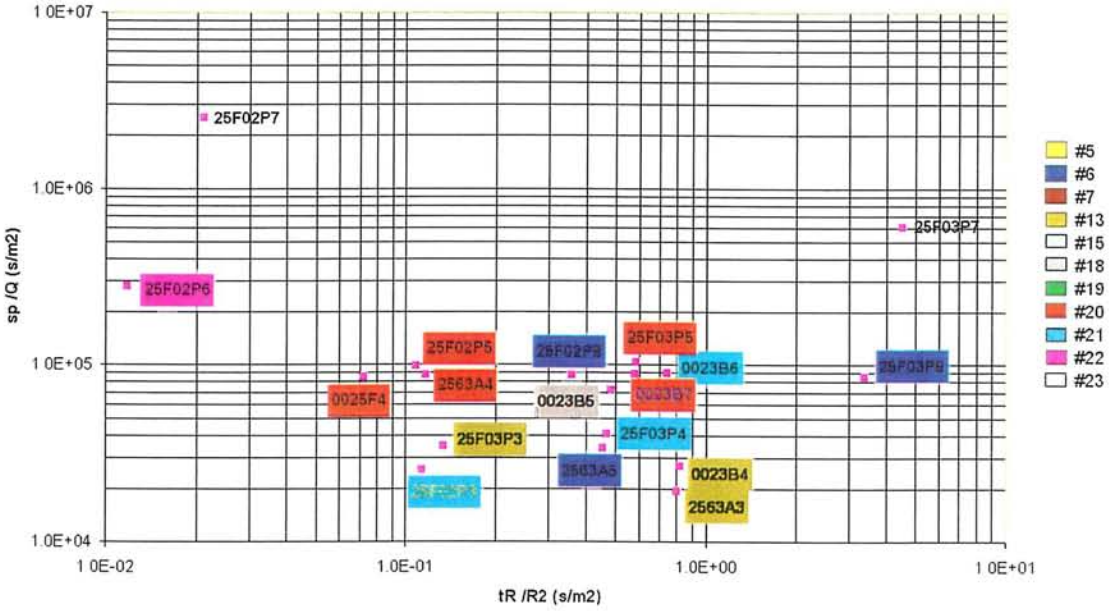

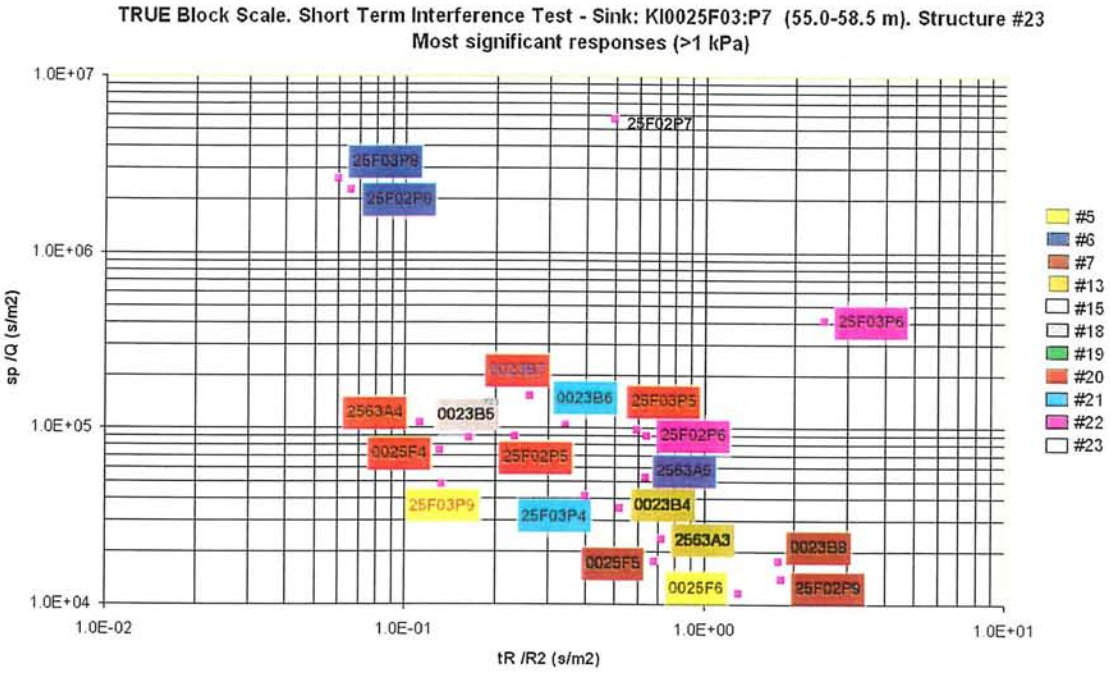
TRUE Block Scale. Short Term Interference Test - Sink: KI0025F03:P7 (55.0-58.5 m). Structure #23
Most significant responses (>1 kPa)
1.0E+07
1.0E+06
1.0E+05
1.0E+04
sp /Q (s/m2)
1.0E-02
1.0E-01
1.0E+00
1.0E+01
tR /R2 (s/m2)
25F02P7
25F03P8
25F02P8
25F03P6
0023B7
0023B6
25F03P5
2563A4
0023B5
25F02P6
0025F4
25F02P5
2563A5
25F03P9
25F03P4
0023B4
2563A3
0023B8
0025F5
0025F6
25F02P9
#5
#6
#7
#13
#15
#18
#19
#20
#21
#22
#23